

Quantum Speed Limit under Calibration Uncertainty

Salman Sajad Wani and Saif Al-Kuwari

Qatar Center for Quantum Computing, College of Science and Engineering, Hamad Bin Khalifa University, Doha, Qatar

Standard quantum speed limits presuppose exactly known parameters, overestimating operational speed under calibration uncertainty. We introduce a projected speed limit based on the quantum Fisher information that profiles out these nuisance parameters on a quotient manifold. We derive constructive bounds for general Markovian evolution using sensitivity equations. Applying this to Jaynes–Cummings sensors, we obtain explicit detuning tolerances and quantify speed limits arising from field-dependent Purcell loss. This framework turns geometric bounds into concrete design rules for calibration and interrogation time.

INTRODUCTION

Quantum speed limit (QSL) quantify the minimal time for a quantum state to evolve into a distinguishable state. The earliest bounds, due to Mandelstam–Tamm and Margolus–Levitin, relate the orthogonalization time to the energy variance and, respectively, to the mean energy above the ground state [1–3]. Geometric treatments recast these results in the Bures/Uhlmann geometry and use the symmetric logarithmic derivative (SLD) quantum Fisher information (QFI) metric to fix the line element [4–7]. Subsequent work extended this framework to general open-system dynamics, yielding QSLs expressed directly in terms of the instantaneous statistical speed for completely positive trace-preserving evolutions [8–10]. Related developments also exploited the nonuniqueness of contractive distinguishability metrics to construct generalized geometric QSL families for unitary and nonunitary dynamics, including bounds that can be tighter than the conventional QFI/Bures choice [11]. For open dynamics, studies have emphasized complementary desiderata such as tightness, robustness under composition and mixing, and computational or experimental feasibility [12]. Related work also sharpened the operational interpretation of quantum speed limits, including in open-system settings [13, 14]. More recent Liouville-space formulations have derived exact and inexact QSL families for completely positive trace-preserving dynamics and clarified attainability for time-optimal CPTP evolutions [15]. These developments have deepened the link between QSLs, quantum estimation theory, and monotone information metrics [7, 16, 17]. They also underpin many analyses of quantum metrology, control, and dissipation [18–20].

A common feature across the standard Bures/QFI setting, generalized geometric families, and more recent open-system and CPTP formulations is the assumption of a fixed, known generator [8–12, 15]. Operationally, distinguishability along laboratory time is therefore confounded by nuisance directions in parameter space: an experimenter can partially compensate for changes in time by co-varying these parameters within their estimation uncertainty. Consequently, the physical Bures

speed computed at a fixed generator generally overestimates the operational speed relevant for distinguishing states modulo nuisance reparametrizations.

In this paper we formulate a nuisance-aware projected quantum speed limit. We treat time and nuisance parameters jointly within the multiparameter SLD-QFI and project the Bures metric onto the time direction via a Schur complement [21–23]. This construction yields an effective information F_{eff} and an associated projected speed $v_{\text{quo}} = \frac{1}{2}\sqrt{F_{\text{eff}}}$. This speed never exceeds the standard Bures speed and remains invariant under reparametrizations of the nuisance manifold. Crucially, F_{eff} coincides with the partial SLD Fisher information, which sets the ultimate precision limit when nuisance parameters are profiled out [24, 25]. In contrast to standard formulations [8–10], which bound evolution for a frozen generator, our framework quantifies operational distinguishability modulo nuisances. We implement this for general Markovian dynamics using GKSL sensitivity equations [19, 20, 26, 27] and analyze two paradigmatic sensors: a unitary Jaynes–Cummings (JC) model and a dispersive JC cavity with loss. For the examples studied here, the nuisance penalty is more pronounced in the dispersive open JC sensor, since the field controls both the coherent cavity-frequency shift and the effective decay rate. In both regimes, the projected QSL converts abstract geometric limits into concrete design rules. One example is the tolerance $|\Delta|t \lesssim 0.3$ for retaining 99% of the physical speed.

FORMALISM

We work in the Bures–SLD geometry of quantum states. The Bures metric, induced by the Uhlmann fidelity, provides the local statistical distance on the space of density operators [4–7]. The corresponding symmetric logarithmic derivative (SLD) operators L_μ are defined by

$$\partial_\mu \rho = \frac{1}{2}(\rho L_\mu + L_\mu \rho), \quad (1)$$

and the associated SLD quantum Fisher information matrix (QFIM) $F_{\mu\nu}$ determines the local line element

$$dL^2 = \frac{1}{4}F_{\mu\nu} dx^\mu dx^\nu. \quad (2)$$

For any parameter direction, this quadratic form gives the local sensitivity of the state to infinitesimal displacements; for time evolution, its square root is the instantaneous statistical speed that underlies geometric quantum speed limits [6, 8, 28]. We take the coordinate vector $x^\mu = (t, \boldsymbol{\lambda})$ to include both laboratory time and the nuisance parameters $\boldsymbol{\lambda}$ (e.g., detunings, loss rates). In our setting, $\boldsymbol{\lambda}$ are not targets of joint estimation but sources of uncertainty. Throughout this work, the nuisance parameters $\boldsymbol{\lambda}$ are treated as run-wise fixed but imperfectly known calibration parameters that label the generator of the dynamics. They are therefore distinct from explicitly time-dependent stochastic fluctuations, which belong to a different modeling layer and are not profiled by the present Schur-complement construction. In this multi-parameter setting, the QFIM takes the block form

$$F = \begin{pmatrix} F_{tt} & \mathbf{f}^\top \\ \mathbf{f} & F_{\lambda\lambda} \end{pmatrix}, \quad \mathbf{f} := (F_{t\alpha})_\alpha, \quad F_{\lambda\lambda} := (F_{\alpha\beta})_{\alpha,\beta}. \quad (3)$$

Standard ‘‘physical’’ QSLs are obtained by fixing $\boldsymbol{\lambda}$ and using F_{tt} alone. Operationally, however, an experimenter can re-tune $\boldsymbol{\lambda}$ to reduce distinguishability along nuisance directions. Thus the relevant speed is set not by F_{tt} , but by the information component that is orthogonal to the nuisance manifold.

To isolate this component, we minimize dL^2 over $d\boldsymbol{\lambda}$ at fixed dt , profiling the Bures quadratic form in analogy with profile likelihood [21, 22, 29]. Solving the normal equations yields the Schur complement

$$F_{\text{eff}} := F_{tt} - \mathbf{f}^\top F_{\lambda\lambda}^{-1} \mathbf{f}, \quad (4)$$

where $F_{\lambda\lambda}^{-1}$ denotes the Moore–Penrose pseudoinverse on the estimable nuisance subspace [23, 30]. Geometrically, this Schur complement is the squared norm of the time tangent after orthogonal projection away from the nuisance directions in the Bures–SLD geometry. It therefore removes the distinguishability attributable to nuisance reparametrizations. Equivalently, the profiled quadratic form induces the local quotient metric obtained by identifying tangent variations that differ only by nuisance components: $dL_{\text{quo}}^2 = 1/4 F_{\text{eff}} dt^2$. F_{eff} satisfies $0 \leq F_{\text{eff}} \leq F_{tt}$ and is invariant under smooth reparametrizations of $\boldsymbol{\lambda}$. When F is invertible, $F_{\text{eff}} = ((F^{-1})_{tt})^{-1}$, recovering the standard profiled information. Rank-deficient states (including pure states) are handled by restricting all constructions to $\text{supp}(\rho)$ [16, 31].

In the SLD formalism, F_{eff} coincides with the partial quantum Fisher information for time. Projecting L_t orthogonally to the span of nuisance scores $\{L_\alpha\}$ via the inner product $\langle\langle A, B \rangle\rangle_\rho := \frac{1}{2} \text{Tr}[\rho\{A, B\}]$ yields the efficient score \tilde{L}_t , whose norm is

$$\langle\langle \tilde{L}_t, \tilde{L}_t \rangle\rangle_\rho = F_{tt} - \mathbf{f}^\top F_{\lambda\lambda}^{-1} \mathbf{f} = F_{\text{eff}}. \quad (5)$$

Thus, the projected metric coefficient sets the ultimate

precision limit $\text{Var}(\hat{t}) \geq 1/(NF_{\text{eff}})$ attainable when nuisance parameters are profiled out [24, 25].

To embed this geometry into Markovian dynamics, we consider trajectories generated by the GKSL master equation

$$\partial_t \rho(t, \boldsymbol{\lambda}) = \mathcal{L}_\lambda[\rho] := -\frac{i}{\hbar} [H(\boldsymbol{\lambda}), \rho] + \sum_k \mathcal{D}[F_k(\boldsymbol{\lambda})]\rho. \quad (6)$$

The time derivative entering the QFIM is $\partial_t \rho = \mathcal{L}_\lambda[\rho]$, while the nuisance derivatives $\rho'_\alpha := \partial_{\lambda_\alpha} \rho$ satisfy the linear sensitivity equation

$$\partial_t \rho'_\alpha(t) = (\partial_{\lambda_\alpha} \mathcal{L}_\lambda)[\rho(t)] + \mathcal{L}_\lambda[\rho'_\alpha(t)]. \quad (7)$$

This equation allows $F_{\text{eff}}(t)$ to be evaluated efficiently along any trajectory using the Duhamel formula [26, 27]. At each fixed time, the profiling step remains explicit: one solves the normal equations $F_{\lambda\lambda} d\boldsymbol{\lambda}_* = -\mathbf{f} dt$ and substitutes the result into the quadratic form, recovering the same Schur complement as above. The effective information defines the instantaneous projected speed $v_{\text{quo}}(t) := \frac{1}{2} \sqrt{F_{\text{eff}}(t)}$. Its time integral is the quotient length of the realized path, while the global minimization is already contained in the quotient geodesic distance $L_{\text{quo}}([\rho_0], [\rho_\tau])$. Integrating this speed yields the projected quantum speed limit

$$\tau \geq \frac{L_{\text{quo}}([\rho_0], [\rho_\tau])}{\bar{v}_{\text{quo}}}, \quad \bar{v}_{\text{quo}} := \frac{1}{\tau} \int_0^\tau \frac{1}{2} \sqrt{F_{\text{eff}}(t)} dt, \quad (8)$$

where L_{quo} is the geodesic distance between equivalence classes $[\rho]$ on the quotient manifold. In the absence of nuisances ($F_{t\alpha} = 0$), this reduces to standard QFI-based bounds [8–10]. For unitary dynamics, it yields a Mandelstam–Tamm–type bound governed by an effective variance Δ_{eff} [1, 2] (see Appendix A). The projected QSL is saturated when the realized evolution, viewed in the quotient geometry obtained after profiling out nuisance directions, is a minimizing geodesic between the endpoint equivalence classes. Equivalently,

$$L_{\text{quo}}([\rho_0], [\rho_\tau]) = \int_0^\tau \frac{1}{2} \sqrt{F_{\text{eff}}(t)} dt. \quad (9)$$

When $F_{t\alpha} = 0$, one has $F_{\text{eff}} = F_{tt}$, so the projected-QSL denominator coincides with the standard geometric denominator. If the realized endpoint also attains the quotient optimization over the admissible nuisance values, then the quotient endpoint distance coincides with the physical Bures distance for that run, and the saturation question reduces to the usual one for the underlying dynamics.

UNITARY EXAMPLE: JAYNES–CUMMINGS SENSOR.

We first illustrate the projected QSL in a setting where estimation and dynamics are statistically correlated: a

Jaynes–Cummings (JC) qubit–cavity sensor for a magnetic field B [32–34]. Within the rotating–wave approximation and restricted to the single–excitation manifold $\{|e, 0\rangle, |g, 1\rangle\}$, the dynamics is generated by the traceless Hamiltonian

$$H'(B) = g\tau_x + \frac{\Delta(B)}{2}\tau_z, \quad \Delta(B) = \omega_q + \gamma B - \omega_c, \quad (10)$$

with associated Rabi frequency $\Omega = \sqrt{\Delta^2 + 4g^2}$. We initialize in $|\psi_0\rangle = |e, 0\rangle$ and treat the field B , through the detuning $\Delta(B)$, as a nuisance parameter.

For a pure state $|\psi(x)\rangle = U(x)|\psi_0\rangle$, the QFIM is given by the covariance of the local generators, $F_{\mu\nu} = 4\text{Cov}_{\psi_0}(G_\mu, G_\nu)$ [6]. Here the time generator is $G_t = H'(B)$, while the field generator $G_B(t)$ is dynamical because $[H', \partial_B H'] \neq 0$. An explicit evaluation of the Heisenberg equations (see Appendix B) yields

$$F_{tt} = 4g^2, \quad (11a)$$

$$F_{tB}(t) = \frac{4g^2\gamma\Delta}{\Omega^2} \left(t - \frac{\sin\Omega t}{\Omega} \right), \quad (11b)$$

so that the diagonal element F_{tt} reproduces the standard Mandelstam–Tamm speed $v_{\text{phys}} = 2g$, while the nonzero off–diagonal term F_{tB} captures the correlation between time evolution and field uncertainty.

Eliminating the field uncertainty via the Schur complement $F_{\text{eff}} = F_{tt} - F_{tB}^2/F_{BB}$ yields the effective information

$$F_{\text{eff}}(t) = 4g^2 \frac{4\sin^4(\frac{\Omega t}{2})}{\Delta^2(t - \frac{\sin\Omega t}{\Omega})^2 + 4\sin^4(\frac{\Omega t}{2})}. \quad (12)$$

Two regimes are particularly instructive. (i) At exact resonance ($\Delta = 0$), the correlation F_{tB} vanishes and the projected speed coincides with the physical speed. (ii) For small detunings and short times ($|\Omega t| \ll 1$), a Taylor expansion gives a quadratic penalty:

$$\frac{F_{\text{eff}}(t)}{F_{tt}} \approx \frac{1}{1 + (\Delta t/3)^2} \simeq 1 - \frac{(\Delta t)^2}{9}. \quad (13)$$

Thus, even a modest residual detuning reduces the operational speed v_{quo} below the naive Mandelstam–Tamm value.

This reduction leads directly to quantitative design rules. If we require the projected speed to retain a fraction R of the physical speed, we obtain the tolerance

$$|\Delta|t < 3\sqrt{\frac{1}{R} - 1}. \quad (14)$$

For example, keeping $R = 0.99$ requires $|\Delta|t < 0.30$. This inequality shows how tightly the JC sensor must be kept near resonance for the operational QSL to remain close to the QSL computed at fixed generator. Profiling nuisance parameters therefore turns the geometric construction into concrete constraints on calibration effort and on the admissible (Δ, τ) working window (see Fig. 1).

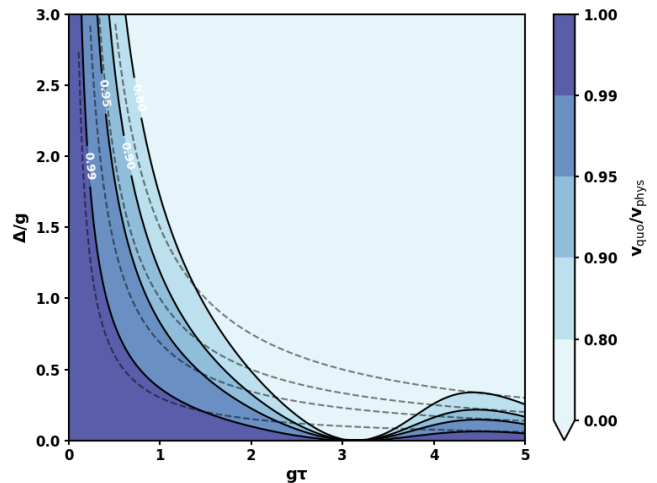


FIG. 1. **Calibration phase diagram for the unitary Jaynes–Cummings sensor.** The heatmap shows the ratio of projected to physical speed, $\mathcal{R} = v_{\text{quo}}/v_{\text{phys}}$, as a function of the dimensionless interrogation time $g\tau$ and the normalized detuning Δ/g . White solid contours mark the retention levels $R = 0.99, 0.95, 0.90$, and 0.80 . Black dashed curves show the analytical tolerance $|\Delta|\tau \approx 3\sqrt{1/R - 1}$ derived in Eq. (14). The dark blue region marks the admissible (Δ, τ) working window in which nuisance profiling has only a small effect on the operational quantum speed.

OPEN EXAMPLE: DISPERSIVE JC SENSOR WITH LOSS.

We next consider a realistic sensor with noisy, parameter-dependent dynamics: a Jaynes–Cummings cavity coupled to a two-level atom, operated in the dispersive regime ($\Delta \gg g$) [32, 35]. Here the dissipation is modeled by a Markovian master equation for fixed B , while the uncertainty in B itself is treated as static calibration uncertainty during a given run. The atom acts as a probe for the field B , shifting the cavity frequency via the AC Stark effect and at the same time introducing dissipation.

By applying a Schrieffer–Wolff transformation [35, 36] and tracing out the fast-relaxing atom (see Appendix C), we obtain an effective master equation for the cavity mode ρ_{cav} :

$$\dot{\rho}_{\text{cav}} = -i[\omega'_c(B)\tilde{a}^\dagger\tilde{a}, \rho_{\text{cav}}] + \kappa_{\text{eff}}(B)\mathcal{D}[\tilde{a}]\rho_{\text{cav}}. \quad (15)$$

In the dispersive regime, the Schrieffer–Wolff transformation removes the off-resonant atom–cavity exchange term order by order in $g/\Delta(B)$ and leaves a dressed cavity mode whose resonance is shifted by virtual atomic excitations. The same dressing admixes a small atomic component into the effective cavity excitation, so atomic relaxation is inherited by the cavity as an additional decay channel, yielding the field-dependent Purcell contribution to $\kappa_{\text{eff}}(B)$ [37]. Hence the same parameter B

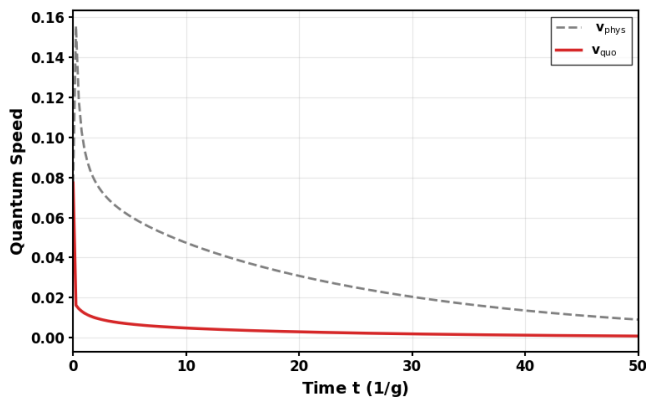


FIG. 2. **Operational speed penalty from Purcell-enhanced loss.** The figure shows the instantaneous physical speed v_{phys} (gray dashed) and projected speed v_{quo} (red solid) for a dispersive Jaynes–Cummings sensor with parameters $\Delta = 8g$, $\kappa = 0.05g$, and $\gamma_1 = 2g$. Whereas the physical speed remains high because the state continues to decay dissipatively, the projected speed shows a pronounced nuisance penalty driven by the statistical correlation between time and the field-dependent decay rates.

controls both the coherent signal, carried by the field-pulled frequency $\omega'_c(B)$, and the dissipative envelope, through the effective decay rate $\kappa_{\text{eff}}(B) = \kappa + \delta\kappa(B)$. This joint dependence is the physical origin of the trade-off in Fig. 2: increasing the dispersive response simultaneously strengthens the loss channel, which makes the passage of time more easily mimicked by a change in the field-dependent decay rate and therefore increases the nuisance penalty in the projected speed. For an initial superposition state, the evolved density matrix takes the Bloch form $\rho_{\text{cav}}(t) = \frac{1}{2}(\mathbb{I} + \vec{S} \cdot \boldsymbol{\sigma})$. The Bloch components then evolve as

$$\begin{aligned} S_x &= \sin(2\theta) \cos[\omega'_c(B)t] e^{-\kappa_{\text{eff}}(B)t/2}, \\ S_y &= -\sin(2\theta) \sin[\omega'_c(B)t] e^{-\kappa_{\text{eff}}(B)t/2}, \\ S_z &= 2\sin^2\theta e^{-\kappa_{\text{eff}}(B)t} - 1. \end{aligned} \quad (16)$$

Accordingly, the parameter B enters both the oscillation frequency and the exponential decay envelope. The effective information $F_{\text{eff}}(t) = F_{tt} - F_{tB}^2/F_{BB}$ quantifies the balance between coherent phase accumulation and irreversible amplitude decay.

These effects are summarized in Fig. 2. The physical speed v_{phys} simply tracks the continuous decay of the state, whereas the projected speed v_{quo} falls off rapidly and reveals a growing nuisance penalty. This divergence arises because photon loss is statistically confounded with uncertainty in B : an experimenter cannot tell whether a weaker signal is caused by the passage of time or by a change in the Purcell rate.

To bound the evolution, we compute the quotient fi-

delity by maximizing over the calibration window \mathcal{B} :

$$\Theta_{\text{quo}}(\tau) := \arccos\left(\sup_{B \in \mathcal{B}} \sqrt{F(\rho_0, \rho_{\text{cav}}(\tau; B))}\right). \quad (17)$$

Combining this with the averaged projected speed gives the open-system bound $\tau \geq \Theta_{\text{quo}}/\bar{v}_{\text{quo}}$. This result identifies a finite optimal interrogation time, before the nuisance penalty dominates. In this way, the geometric limit becomes a concrete design rule for dispersive readout [35, 38].

CONCLUSION

We introduced a nuisance-aware quantum speed limit on the quotient manifold of physical states, which identifies trajectories that differ only by unobservable reparametrizations of the generator. Projecting the multiparameter Bures metric via the Schur complement [21, 22] yields an operational speed v_{quo} , which provides a lower bound on distinguishability in the presence of calibration uncertainty. Unlike standard QSLs that assume a fixed generator [8, 9], this framework captures the statistical confounding between time evolution and nuisance parameters.

By embedding Markovian dynamics into this geometry, we turn abstract information-geometric limits into concrete design rules. As demonstrated for the unitary and dissipative Jaynes–Cummings sensors, the projected QSL sets explicit experimental tolerances—such as the detuning limit $|\Delta|t \lesssim 0.3$ and the Purcell-penalty cut-off—needed to approach fundamental physical bounds. This shift from kinematic constraints to operational benchmarks enables nuisance-profiled metrology in complex architectures and ties idealized geometric theorems to the noisy, uncertain behavior of real quantum hardware.

-
- [1] L. Mandelstam and I. Tamm, The uncertainty relation between energy and time in non-relativistic quantum mechanics, *J. Phys. (USSR)* **9**, 249 (1945).
 - [2] J. Anandan and Y. Aharonov, Geometry of quantum evolution, *Phys. Rev. Lett.* **65**, 1697 (1990).
 - [3] N. Margolus and L. B. Levitin, The maximum speed of dynamical evolution, *Physica D* **120**, 188 (1998).
 - [4] D. Bures, An extension of kakutani’s theorem on infinite product measures, *Transactions of the American Mathematical Society* **135**, 199 (1969).
 - [5] A. Uhlmann, The “transition probability” in the state space of a $*$ -algebra, *Rep. Math. Phys.* **9**, 273 (1976).
 - [6] S. L. Braunstein and C. M. Caves, Statistical distance and the geometry of quantum states, *Phys. Rev. Lett.* **72**, 3439 (1994).
 - [7] D. Petz, Monotone metrics on matrix spaces, *Linear Algebra Appl.* **244**, 81 (1996).

- [8] M. M. Taddei, B. M. Escher, L. Davidovich, and R. L. de Matos Filho, Quantum speed limit for physical processes, *Phys. Rev. Lett.* **110**, 050402 (2013).
- [9] A. del Campo, I. L. Egusquiza, M. B. Plenio, and S. F. Huelga, Quantum speed limits in open system dynamics, *Phys. Rev. Lett.* **110**, 050403 (2013).
- [10] S. Deffner and E. Lutz, Quantum speed limit for non-markovian dynamics, *Phys. Rev. Lett.* **111**, 010402 (2013).
- [11] D. P. Pires, M. Cianciaruso, L. C. Céleri, G. Adesso, and D. O. Soares-Pinto, Generalized geometric quantum speed limits, *Physical Review X* **6**, 021031 (2016).
- [12] F. Campaioli, F. A. Pollock, and K. Modi, Tight, robust, and feasible quantum speed limits for open dynamics, *Quantum* **3**, 168 (2019).
- [13] E. O'Connor, G. Guarnieri, and S. Campbell, Action quantum speed limits, *Physical Review A* **103**, 022210 (2021).
- [14] Y. Shao, B. Liu, M. Zhang, H. Yuan, and J. Liu, Operational definition of a quantum speed limit, *Physical Review Research* **2**, 023299 (2020).
- [15] A. Srivastav, V. Pandey, B. Mohan, and A. K. Pati, Family of exact and inexact quantum speed limits for completely positive and trace-preserving dynamics, *Physical Review A* **112**, 052204 (2025).
- [16] C. W. Helstrom, *Quantum Detection and Estimation Theory* (Academic Press, New York, 1976).
- [17] D. Petz and C. Sudár, Geometries of quantum states, *J. Math. Phys.* **37**, 2662 (1996).
- [18] V. Giovannetti, S. Lloyd, and L. Maccone, Advances in quantum metrology, *Nat. Photonics* **5**, 222 (2011).
- [19] G. Lindblad, On the generators of quantum dynamical semigroups, *Commun. Math. Phys.* **48**, 119 (1976).
- [20] V. Gorini, A. Kossakowski, and E. C. G. Sudarshan, Completely positive dynamical semigroups of n -level systems, *J. Math. Phys.* **17**, 821 (1976).
- [21] D. R. Cox and N. Reid, Parameter orthogonality and approximate conditional inference, *J. R. Stat. Soc. Ser. B* **49**, 1 (1987).
- [22] S. M. Kay, *Fundamentals of Statistical Signal Processing, Volume I: Estimation Theory* (Prentice Hall, Englewood Cliffs, NJ, 1993).
- [23] F. Zhang, ed., *The Schur Complement and Its Applications*, Numerical Methods and Algorithms, Vol. 4 (Springer, New York, 2005).
- [24] J. Suzuki, Nuisance parameter problem in quantum estimation theory: Tradeoff relation and qubit examples, *Journal of Physics A: Mathematical and Theoretical* **53**, 264001 (2020), arXiv:1905.04733 [quant-ph].
- [25] J. S. Sidhu and P. Kok, Geometric perspective on quantum parameter estimation, *AVS Quantum Science* **2**, 014701 (2020), arXiv:1908.08904 [quant-ph].
- [26] A. Pazy, *Semigroups of Linear Operators and Applications to Partial Differential Equations* (Springer, New York, 1983).
- [27] K.-J. Engel and R. Nagel, *One-Parameter Semigroups for Linear Evolution Equations* (Springer, New York, 2000).
- [28] S. Deffner and S. Campbell, Quantum speed limits: from Heisenberg's uncertainty principle to optimal quantum control, *J. Phys. A: Math. Theor.* **50**, 453001 (2017).
- [29] S.-i. Amari and H. Nagaoka, *Methods of Information Geometry*, Translations of Mathematical Monographs, Vol. 191 (American Mathematical Society / Oxford University Press, Providence, RI, 2000).
- [30] A. Ben-Israel and T. N. E. Greville, *Generalized Inverses: Theory and Applications*, 2nd ed. (Springer, New York, 2003).
- [31] D. Šafránek, Discontinuities of the quantum fisher information and the bures metric, *Phys. Rev. A* **95**, 052320 (2017).
- [32] E. T. Jaynes and F. W. Cummings, Comparison of quantum and semiclassical radiation theories with application to the beam maser, *Proc. IEEE* **51**, 89 (1963).
- [33] C. W. Gardiner and P. Zoller, *Quantum Noise*, 3rd ed. (Springer, Berlin, 2004).
- [34] H. J. Carmichael, *An Open Systems Approach to Quantum Optics*, Lecture Notes in Physics m18 (Springer, Berlin, 1993).
- [35] A. Blais, R.-S. Huang, A. Wallraff, S. M. Girvin, and R. J. Schoelkopf, Cavity quantum electrodynamics for superconducting electrical circuits: An architecture for quantum computation, *Phys. Rev. A* **69**, 062320 (2004).
- [36] J. R. Schrieffer and P. A. Wolff, Relation between the anderson and kondo hamiltonians, *Phys. Rev.* **149**, 491 (1966).
- [37] E. M. Purcell, Spontaneous emission probabilities at radio frequencies, *Phys. Rev.* **69**, 681 (1946).
- [38] J. Gambetta, A. Blais, D. I. Schuster, A. Wallraff, L. Frunzio, J. Majer, M. H. Devoret, S. M. Girvin, and R. J. Schoelkopf, Qubit-photon interactions in a cavity: Measurement-induced dephasing and number splitting, *Phys. Rev. A* **74**, 042318 (2006).
- [39] V. Gorini, A. Kossakowski, and E. C. G. Sudarshan, Completely positive dynamical semigroups of n -level systems, *Journal of Mathematical Physics* **17**, 821 (1976).
- [40] H.-P. Breuer and F. Petruccione, *The Theory of Open Quantum Systems* (Oxford University Press, Oxford, 2002).
- [41] M. Hübner, Computation of uhlmann's parallel transport for density matrices and the bures metric tensor, *Physics Letters A* **163**, 239 (1992).
- [42] J. Dittmann, On the riemannian metric on the space of density matrices, *Physics Letters A* **257**, 87 (1999).
- [43] R. A. Horn and C. R. Johnson, *Matrix Analysis*, 2nd ed. (Cambridge University Press, Cambridge, 2013).
- [44] I. Bengtsson and K. Życzkowski, *Geometry of Quantum States: An Introduction to Quantum Entanglement* (Cambridge University Press, Cambridge, 2006).
- [45] A. Pazy, *Semigroups of Linear Operators and Applications to Partial Differential Equations* (Springer, New York, 1983).
- [46] D. Safránek, Simple expression for the quantum fisher information matrix, *Physical Review A* **97**, 042322 (2018).

APPENDIX A: DETAILED FORMALISM — BURES GEOMETRY, SCHUR COMPLEMENT, AND GKSL DYNAMICS

In this section we derive, in full detail, the geometric quantities and constructions used in the main text: the Bures metric and SLD quantum Fisher information matrix (QFIM), the Schur-complement projection that profiles out nuisance parameters, and the embedding of Markovian dynamics via GKSL sensitivity equations. This provides the rigorous backbone for the projected (quotient) quantum speed limit used in Sec. II of the main text.

Throughout we work on a finite-dimensional Hilbert space \mathcal{H} . Parameters are real and collected as

$$x^\mu = (t, \lambda^1, \dots, \lambda^{m-1}) \in \mathbb{R}^m, \quad (\text{A1})$$

with C^1 dependence of the state family $\rho(x)$ and of the GKSL data $H(\boldsymbol{\lambda}), \{F_k(\boldsymbol{\lambda})\}$.

Setting and GKSL dynamics

For each fixed $\boldsymbol{\lambda}$, the laboratory time evolution is generated by a time-independent GKSL (Lindblad) generator

$$\partial_t \rho(t, \boldsymbol{\lambda}) = \mathcal{L}_{\boldsymbol{\lambda}}[\rho] := -\frac{i}{\hbar} [H(\boldsymbol{\lambda}), \rho] + \sum_k \left(F_k \rho F_k^\dagger - \frac{1}{2} \{F_k^\dagger F_k, \rho\} \right). \quad (\text{A2})$$

See Refs. [19, 39, 40]. Normalization $\text{Tr} \rho(t, \boldsymbol{\lambda}) = 1$ implies that for any tangent $\delta\rho$ one has $\text{Tr}(\delta\rho) = 0$.

Our goal in this section is to start from the Uhlmann fidelity, derive the Bures metric and the SLD-QFIM, project away nuisance directions by a Schur complement to obtain an effective (profiled) information F_{eff} , and then combine this with the GKSL dynamics (A2) to obtain a projected (quotient) quantum speed limit.

From Uhlmann fidelity to the Bures metric

The Uhlmann fidelity between two density operators ρ and σ is defined as

$$F_U(\rho, \sigma) := \left(\text{Tr} \sqrt{\sqrt{\rho} \sigma \sqrt{\rho}} \right)^2. \quad (\text{A3})$$

For nearby states $\sigma = \rho + \delta\rho$, the fidelity admits the expansion

$$F_U(\rho, \rho + \delta\rho) = 1 - g_\rho(\delta\rho, \delta\rho) + o(\|\delta\rho\|^2), \quad (\text{A4})$$

which defines the Bures metric tensor g_ρ [4, 5, 41, 42].

To make this explicit, let ρ be full rank (the rank-deficient case is handled below in the subsection ‘‘Rank-deficient states and singular nuisance blocks’’), with spectral decomposition equation A

$$\rho = \sum_i p_i |i\rangle \langle i|, \quad p_i > 0. \quad (\text{A5})$$

Set

$$\sigma = \rho + \delta\rho, \quad \mathcal{A} := \sqrt{\rho} \sigma \sqrt{\rho} = \rho^2 + \sqrt{\rho} \delta\rho \sqrt{\rho}, \quad (\text{A6})$$

and define the positive square root

$$\mathcal{M} := \sqrt{\mathcal{A}}. \quad (\text{A7})$$

We expand \mathcal{M} in powers of $\delta\rho$:

$$\mathcal{M} = \rho + X + Y + O(\|\delta\rho\|^3), \quad (\text{A8})$$

where $X = O(\delta\rho)$ collects linear terms and $Y = O(\delta\rho^2)$ collects quadratic terms. The defining identity $\mathcal{M}^2 = \mathcal{A}$ then yields two Sylvester equations:

$$\rho X + X \rho = \sqrt{\rho} \delta\rho \sqrt{\rho}, \quad (\text{A9})$$

$$\rho Y + Y \rho = -X^2. \quad (\text{A10})$$

See, e.g., [41–43].

In the eigenbasis of ρ , the solution of (A9) is

$$X_{ij} = \frac{\sqrt{p_i p_j}}{p_i + p_j} (\delta\rho)_{ij}, \quad \text{Tr } X = \frac{1}{2} \text{Tr}(\delta\rho) = 0, \quad (\text{A11})$$

where we used $\text{Tr}(\delta\rho) = 0$. To obtain $\text{Tr } Y$, we work with (A10). Taking the trace in the eigenbasis,

$$\text{Tr } Y = -\frac{1}{2} \text{Tr}(\rho^{-1} X^2) = -\frac{1}{2} \sum_{i,j} \frac{p_j}{(p_i + p_j)^2} |(\delta\rho)_{ij}|^2. \quad (\text{A12})$$

Using symmetry under $i \leftrightarrow j$,

$$\begin{aligned} \sum_{i,j} \frac{p_j}{(p_i + p_j)^2} |(\delta\rho)_{ij}|^2 &= \frac{1}{2} \sum_{i,j} \frac{p_i + p_j}{(p_i + p_j)^2} |(\delta\rho)_{ij}|^2 \\ &= \frac{1}{2} \sum_{i,j} \frac{|(\delta\rho)_{ij}|^2}{p_i + p_j}, \end{aligned} \quad (\text{A13})$$

so that

$$\text{Tr } Y = -\frac{1}{4} \sum_{i,j} \frac{|(\delta\rho)_{ij}|^2}{p_i + p_j}. \quad (\text{A14})$$

Next, expand the square root of the fidelity. By definition,

$$\sqrt{F_U(\rho, \sigma)} = \text{Tr} \sqrt{\mathcal{A}} = \text{Tr } \mathcal{M}. \quad (\text{A15})$$

Using $\text{Tr } \rho = 1$ and $\text{Tr } X = 0$, we find

$$\sqrt{F_U(\rho, \rho + \delta\rho)} = 1 + \text{Tr } Y + O(\|\delta\rho\|^3) = 1 - \frac{1}{4} \sum_{i,j} \frac{|(\delta\rho)_{ij}|^2}{p_i + p_j} + o(\|\delta\rho\|^2), \quad (\text{A16})$$

where we used (A14). Since $F_U = (\sqrt{F_U})^2$, the second-order expansion of F_U is

$$F_U(\rho, \rho + \delta\rho) = 1 - \frac{1}{2} \sum_{i,j} \frac{|(\delta\rho)_{ij}|^2}{p_i + p_j} + o(\|\delta\rho\|^2). \quad (\text{A17})$$

Comparing with the defining expansion (A4), we obtain the explicit Bures metric tensor

$$g_\rho(\delta\rho, \delta\rho) = \frac{1}{2} \sum_{i,j} \frac{|(\delta\rho)_{ij}|^2}{p_i + p_j}, \quad (\text{A18})$$

as given, e.g., in Refs. [17, 41, 44].

SLD representation and the SLD-QFIM

We now rewrite the metric (A18) in terms of the symmetric logarithmic derivative (SLD). For any tangent $\delta\rho$, the SLD $L(\delta\rho)$ is defined by the Sylvester equation

$$\delta\rho = \frac{1}{2}(\rho L + L\rho) \iff L = J_\rho^{-1}(\delta\rho), \quad J_\rho(X) := \frac{1}{2}(\rho X + X\rho). \quad (\text{A19})$$

In the eigenbasis of ρ ,

$$L_{ij} = \frac{2(\delta\rho)_{ij}}{p_i + p_j}. \quad (\text{A20})$$

Substituting (A20) into (A18) and simplifying, one obtains

$$\begin{aligned}
g_\rho(\delta\rho, \delta\rho) &= \frac{1}{2} \sum_{i,j} \frac{|(\delta\rho)_{ij}|^2}{p_i + p_j} \\
&= \frac{1}{2} \sum_{i,j} \frac{1}{p_i + p_j} \left| \frac{p_i + p_j}{2} L_{ij} \right|^2 \\
&= \frac{1}{8} \sum_{i,j} (p_i + p_j) |L_{ij}|^2 \\
&= \frac{1}{4} \sum_{i,j} p_i |L_{ij}|^2 = \frac{1}{4} \text{Tr}(\rho L^2).
\end{aligned} \tag{A21}$$

Here we used symmetry under $i \leftrightarrow j$ and the Hermiticity of L . Equation (A21) is the standard SLD representation of the Bures metric [6, 7, 16].

We now introduce coordinates $x^\mu = (t, \lambda^1, \dots, \lambda^{m-1})$ on the parameter manifold and expand

$$\delta\rho = \partial_\mu \rho dx^\mu. \tag{A22}$$

Define the coordinate SLD operators L_μ by

$$\partial_\mu \rho = \frac{1}{2}(\rho L_\mu + L_\mu \rho), \quad L_\mu := J_\rho^{-1}(\partial_\mu \rho). \tag{A23}$$

By bilinearity of g_ρ , the Bures line element can be written as

$$\begin{aligned}
dL^2 &= g_\rho(\delta\rho, \delta\rho) = \frac{1}{4} \text{Tr}[\rho(\delta L)^2] \\
&= \frac{1}{4} \text{Tr}[\rho(L_\mu L_\nu)] dx^\mu dx^\nu,
\end{aligned} \tag{A24}$$

where we used $\delta L = L_\mu dx^\mu$. This identifies the SLD QFIM $F_{\mu\nu}$ via

$$dL^2 = \frac{1}{4} F_{\mu\nu} dx^\mu dx^\nu, \quad F_{\mu\nu} := \frac{1}{2} \text{Tr}[\rho(L_\mu L_\nu + L_\nu L_\mu)]. \tag{A25}$$

Since the SLDs are Hermitian, the SLD-QFIM can equivalently be written as the real part of the unsymmetrized trace:

$$F_{\mu\nu} = \frac{1}{2} \text{Tr}[\rho(L_\mu L_\nu + L_\nu L_\mu)] = \text{Re} \text{Tr}(\rho L_\mu L_\nu). \tag{A26}$$

In particular, when $\text{Tr}(\rho L_\mu L_\nu)$ is real for the parameter pair under consideration, the real-part symbol may be omitted.

Using (A19) and (A23), one also obtains a computational expression that is convenient for open-system dynamics:

$$F_{\mu\nu} = 2 \text{Tr}[(\partial_\mu \rho) J_\rho^{-1}(\partial_\nu \rho)]. \tag{A27}$$

Equations (A25) and (A27) are the standard SLD-QFIM formulas [6, 7, 16, 44].

Projecting nuisance directions: Schur complement

We now treat time t and the nuisance parameters $\boldsymbol{\lambda}$ on equal footing as coordinates of the parameter manifold, and then project out the nuisance directions.

Split the indices $\mu = (t, \alpha)$ and block the QFIM as

$$F = \begin{pmatrix} F_{tt} & \mathbf{f}^\top \\ \mathbf{f} & F_{\lambda\lambda} \end{pmatrix}, \quad \mathbf{f} := (F_{t\alpha})_\alpha, \quad F_{\lambda\lambda} := (F_{\alpha\beta})_{\alpha,\beta}. \tag{A28}$$

The Bures line element (A25) can then be written as the quadratic form

$$dL^2 = \frac{1}{4} \left(F_{tt} dt^2 + 2 \mathbf{f}^\top d\boldsymbol{\lambda} dt + d\boldsymbol{\lambda}^\top F_{\lambda\lambda} d\boldsymbol{\lambda} \right). \tag{A29}$$

For fixed dt , the physically relevant distance along t modulo nuisance reparametrizations is obtained by minimizing (A29) over $d\boldsymbol{\lambda} \in \mathbb{R}^{m-1}$. The normal equations are

$$\frac{\partial}{\partial(d\boldsymbol{\lambda})}(dL^2) = \frac{1}{2}(\mathbf{f} dt + F_{\lambda\lambda}d\boldsymbol{\lambda}) = 0, \quad (\text{A30})$$

which gives

$$F_{\lambda\lambda} d\boldsymbol{\lambda}_* = -\mathbf{f} dt, \quad d\boldsymbol{\lambda}_* = -F_{\lambda\lambda}^{-1} \mathbf{f} dt. \quad (\text{A31})$$

Here $F_{\lambda\lambda}^{-1}$ denotes the inverse of $F_{\lambda\lambda}$ on its range; when $F_{\lambda\lambda}$ is singular, it is understood as the Moore–Penrose pseudoinverse [30, 43].

Substituting $d\boldsymbol{\lambda}_*$ back into (A29) yields the minimal squared distance:

$$\begin{aligned} dL_{\min}^2 &= \frac{1}{4} \left(F_{tt} - 2 \mathbf{f}^\top F_{\lambda\lambda}^{-1} \mathbf{f} + \mathbf{f}^\top F_{\lambda\lambda}^{-1} F_{\lambda\lambda} F_{\lambda\lambda}^{-1} \mathbf{f} \right) dt^2 \\ &= \frac{1}{4} \left(F_{tt} - \mathbf{f}^\top F_{\lambda\lambda}^{-1} \mathbf{f} \right) dt^2. \end{aligned} \quad (\text{A32})$$

This identifies the effective (profiled) Fisher information for time as the Schur complement of the nuisance block:

$$F_{\text{eff}} := F_{tt} - \mathbf{f}^\top F_{\lambda\lambda}^{-1} \mathbf{f}, \quad dL_{\min}^2 = \frac{1}{4} F_{\text{eff}} dt^2. \quad (\text{A33})$$

Since the full QFIM F is positive semidefinite, its Schur complements are positive semidefinite as well [23, 43], so $F_{\text{eff}} \geq 0$.

Invariance and relation to profiled information. Consider a smooth reparametrization of the nuisance manifold $\tilde{\boldsymbol{\lambda}} = \phi(\boldsymbol{\lambda})$ with Jacobian J . The QFIM transforms as $F' = J^{-\top} F J^{-1}$, whence

$$F'_{\lambda\lambda} = J^\top F_{\lambda\lambda} J, \quad (\text{A34})$$

$$\mathbf{f}' = J^\top \mathbf{f}. \quad (\text{A35})$$

It follows that

$$\mathbf{f}'^\top (F'_{\lambda\lambda})^{-1} \mathbf{f}' = \mathbf{f}^\top J (J^\top F_{\lambda\lambda} J)^{-1} J^\top \mathbf{f} \quad (\text{A36})$$

$$= \mathbf{f}^\top F_{\lambda\lambda}^{-1} \mathbf{f}, \quad (\text{A37})$$

and hence F_{eff} is a scalar under nuisance reparametrizations.

If the full QFIM F is invertible, one may also use the block inversion formula [43]:

$$F_{\text{eff}} = ((F^{-1})_{tt})^{-1}, \quad (\text{A38})$$

which is the usual profiled Fisher information for t [29]. Thus F_{eff} coincides with the information for t after profiling (maximizing the likelihood) over the nuisance coordinates.

Embedding GKSL dynamics: sensitivities and QFIM blocks

We now bring the GKSL dynamics (A2) inside the geometric construction. Treat $(t, \boldsymbol{\lambda})$ as independent coordinates, and write

$$d\rho = \partial_t \rho dt + \sum_{\alpha} \partial_{\lambda^\alpha} \rho d\lambda^\alpha \equiv \dot{\rho} dt + \sum_{\alpha} \rho'_\alpha d\lambda^\alpha, \quad (\text{A39})$$

where $\dot{\rho} := \mathcal{L}_{\boldsymbol{\lambda}}[\rho]$ is determined by (A2) and

$$\rho'_\alpha := \partial_{\lambda^\alpha} \rho \quad (\text{A40})$$

is the sensitivity of the state to a change in the nuisance parameter λ^α .

Differentiating the GKSL equation (A2) with respect to λ^α and commuting derivatives (under the assumed smoothness) gives

$$\partial_t \rho'_\alpha(t) = (\partial_{\lambda^\alpha} \mathcal{L}_\lambda)[\rho(t)] + \mathcal{L}_\lambda[\rho'_\alpha(t)]. \quad (\text{A41})$$

This is a linear, inhomogeneous ODE on the operator space. Its solution is given by the Duhamel formula [27, 45]:

$$\rho'_\alpha(t) = e^{t\mathcal{L}_\lambda} \rho'_\alpha(0) + \int_0^t e^{(t-s)\mathcal{L}_\lambda} (\partial_{\lambda^\alpha} \mathcal{L}_\lambda)[\rho(s, \lambda)] ds. \quad (\text{A42})$$

Trace preservation of \mathcal{L}_λ and of $\partial_{\lambda^\alpha} \mathcal{L}_\lambda$ implies that $\text{Tr} \rho'_\alpha(t) = \text{Tr} \rho'_\alpha(0)$; taking $\text{Tr} \rho'_\alpha(0) = 0$ ensures that $\rho'_\alpha(t)$ remains a valid tangent (trace-zero) operator for all t [40, 45].

Using the QFIM expression (A27) with $\partial_t \rho = \mathcal{L}_\lambda[\rho]$ and $\partial_{\lambda^\alpha} \rho = \rho'_\alpha$, we obtain the matrix blocks along a dynamical trajectory:

$$F_{tt}(t) = 2 \text{Tr}[(\mathcal{L}_\lambda \rho) J_\rho^{-1}(\mathcal{L}_\lambda \rho)], \quad (\text{A43})$$

$$F_{t\alpha}(t) = 2 \text{Tr}[(\mathcal{L}_\lambda \rho) J_\rho^{-1}(\rho'_\alpha)], \quad (\text{A44})$$

$$F_{\alpha\beta}(t) = 2 \text{Tr}[\rho'_\alpha J_\rho^{-1}(\rho'_\beta)]. \quad (\text{A45})$$

Substituting these blocks into the Schur complement (A33) yields the effective information $F_{\text{eff}}(t)$ along the laboratory trajectory. This is the quantity that enters the projected quantum speed limit.

Quotient metric and local-to-global projected QSL

We now make explicit the quotient-geometric meaning of the profiled quantity F_{eff} and its relation to the global projected quantum speed limit.

At each state ρ , the nuisance coordinates λ^α generate tangent vectors $\partial_{\lambda^\alpha} \rho$. Their span defines the vertical nuisance subspace

$$\mathcal{V}_\rho := \text{span}\{\partial_{\lambda^\alpha} \rho\}_\alpha. \quad (\text{A46})$$

On a regular patch where this nuisance distribution has constant rank, we define the induced quadratic form on a quotient tangent class $[X]$ by minimizing the ambient Bures metric over vertical shifts:

$$g_{\text{quo}}([X], [X]) := \inf_{V \in \mathcal{V}_\rho} g_\rho(X + V, X + V). \quad (\text{A47})$$

Take now $X = \partial_t \rho$ and write

$$V = \xi^\alpha \partial_{\lambda^\alpha} \rho. \quad (\text{A48})$$

Using the block form of the QFIM, the corresponding Bures quadratic form is

$$4g_\rho(X + V, X + V) = F_{tt} + 2\xi^\alpha F_{t\alpha} + \xi^\alpha \xi^\beta F_{\alpha\beta}. \quad (\text{A49})$$

Minimizing (A49) over ξ^α gives the normal equations

$$F_{\alpha\beta} \xi_*^\beta = -F_{t\alpha}, \quad (\text{A50})$$

and therefore

$$4g_{\text{quo}}([\partial_t \rho], [\partial_t \rho]) = F_{tt} - \mathbf{f}^\top F_{\lambda\lambda}^{-1} \mathbf{f} = F_{\text{eff}}. \quad (\text{A51})$$

Thus the Schur complement F_{eff} is precisely the induced quotient metric coefficient along the time direction.

When $F_{\lambda\lambda}$ is singular, the inverse in (A51) is understood in the Moore–Penrose sense on the estimable nuisance subspace, exactly as in (A33). Because the full QFIM block matrix is positive semidefinite, one has $\mathbf{f} \in \text{Ran}(F_{\lambda\lambda})$, equivalently $\mathbf{f} \perp \ker(F_{\lambda\lambda})$. Hence the Moore–Penrose pseudoinverse yields the correct profiled minimum on the estimable nuisance subspace. Likewise, for rank-deficient states all constructions are understood on $\text{supp}(\rho)$, as discussed in Sec. A.

In the SLD language, the same result can be expressed through orthogonal projection of the time score away from the nuisance-score span. If \tilde{L}_t denotes the orthogonal projection of L_t onto the complement of $\text{span}\{L_\alpha\}$ with respect to the inner product $\langle\langle A, B \rangle\rangle_\rho := \frac{1}{2} \text{Tr}[\rho\{A, B\}]$, then, when the nuisance-score Gram matrix is singular, this projection is understood on the estimable nuisance-score subspace, with coefficients determined by the Moore–Penrose pseudoinverse of $F_{\lambda\lambda}$,

$$\langle\langle \tilde{L}_t, \tilde{L}_t \rangle\rangle_\rho = F_{\text{eff}}. \quad (\text{A52})$$

Hence the profiled Fisher information and the quotient-metric coefficient coincide.

Once this local quotient metric is fixed, the instantaneous projected speed is the norm of the tangent to the realized evolution in the quotient geometry:

$$v_{\text{quo}}(t) = \sqrt{g_{\text{quo}}([\dot{\rho}(t)], [\dot{\rho}(t)])} = \frac{1}{2} \sqrt{F_{\text{eff}}(t)}. \quad (\text{A53})$$

Therefore, along the realized trajectory $t \mapsto \rho(t)$, the quotient path length is

$$\ell_{\text{quo}}[\rho(\cdot)] = \int_0^\tau \frac{1}{2} \sqrt{F_{\text{eff}}(t)} dt. \quad (\text{A54})$$

By definition of geodesic distance in the quotient geometry,

$$L_{\text{quo}}([\rho_0], [\rho_\tau]) \leq \ell_{\text{quo}}[\rho(\cdot)]. \quad (\text{A55})$$

Hence

$$L_{\text{quo}}([\rho_0], [\rho_\tau]) \leq \int_0^\tau \frac{1}{2} \sqrt{F_{\text{eff}}(t)} dt. \quad (\text{A56})$$

This shows that no further optimization of v_{quo} along the realized path is needed. The only additional global minimization is the one already contained in the definition of the quotient geodesic distance L_{quo} itself, namely as the infimum of quotient-path lengths over all curves connecting the endpoint equivalence classes.

Projected speed and quotient quantum speed limit

As established in Sec. A, the instantaneous projected (quotient) speed is

$$v_{\text{quo}}(t) := \frac{dL_{\text{quo}}}{dt} = \frac{1}{2} \sqrt{F_{\text{eff}}(t)}. \quad (\text{A57})$$

and the corresponding integral quotient-QSL is

$$L_{\text{quo}}([\rho_0], [\rho_\tau]) \leq \int_0^\tau \frac{1}{2} \sqrt{F_{\text{eff}}(t)} dt. \quad (\text{A58})$$

Rearranging (A58) gives the time-to-target form used in the main text,

$$\tau \geq \frac{L_{\text{quo}}([\rho_0], [\rho_\tau])}{\bar{v}_{\text{quo}}}, \quad \bar{v}_{\text{quo}} := \frac{1}{\tau} \int_0^\tau \frac{1}{2} \sqrt{F_{\text{eff}}(t)} dt, \quad (\text{A59})$$

where \bar{v}_{quo} is the time-averaged projected speed. This is the form used in the main text.

Remark 1 (Physical vs projected QSLs). The physical QSL (without profiling) pairs the physical Bures distance $L(\rho_0, \rho_\tau)$ with the speed $\frac{1}{2} \sqrt{F_{tt}}$, where F_{tt} is the tt -element of the full QFIM. The projected QSL pairs the quotient distance L_{quo} with the projected speed $\frac{1}{2} \sqrt{F_{\text{eff}}}$. Since $F_{\text{eff}} \leq F_{tt}$ and $L_{\text{quo}} \leq L(\rho_0, \rho_\tau)$ (projection never increases distances), one must not mix distances and speeds from different manifolds, as this can invalidate the bound.

Rank-deficient states and singular nuisance blocks

The derivations above assumed full rank for ρ and invertibility of $F_{\lambda\lambda}$. We now state the precise conditions under which the construction extends to rank-deficient states and singular nuisance blocks.

Lemma 1 (Support restriction and continuous extension). *Let ρ be a density matrix (possibly rank-deficient), and let $\text{supp}(\rho)$ denote its support. Restrict all constructions to $\text{supp}(\rho)$, i.e., regard ρ as a strictly positive operator on $\text{supp}(\rho)$ and define J_ρ and J_ρ^{-1} accordingly. Then the formulas (A18)–(A27), (A28)–(A38), (A41)–(A45), and (A57)–(A59) all hold with this understanding. Moreover, continuity of the fidelity in the trace norm implies that the resulting Bures metric is the continuous extension from $\text{supp}(\rho)$ to \mathcal{H} .*

A detailed discussion of these support issues for the Bures metric and the SLD–QFIM can be found in Ref. [46].

Remark 2 (Singular $F_{\lambda\lambda}$). When the nuisance block $F_{\lambda\lambda}$ is singular, the Schur complement (A33) is defined using the Moore–Penrose pseudoinverse $F_{\lambda\lambda}^+$. This yields the unique minimizer on the estimable nuisance subspace and preserves invariance under reparametrizations of the nuisance manifold [23, 30].

APPENDIX B: CLOSED JAYNES–CUMMINGS SENSOR — UNITARY PROJECTED QSL

In this section we specialize the general formalism of Appendix A to a closed Jaynes–Cummings (JC) sensor driven by a static magnetic field. We (i) reduce the model to a two-level single-excitation manifold; (ii) compute the local generators for laboratory time t and field B ; (iii) evaluate the two-parameter QFIM $\{F_{tt}, F_{tB}, F_{BB}\}$ exactly; (iv) form the Schur-complement effective information $F_{\text{eff}}(t)$; and (v) relate these quantities to the fidelity and the projected (quotient) quantum speed limit. Finally, we derive a short-time expansion that yields explicit detuning tolerances for retaining a given fraction of the physical speed.

Model and reduction to the single-excitation manifold

We consider a single-mode cavity of frequency ω_c coupled to a two-level system (atom or qubit) of bare transition frequency ω_q and a magnetic-field-dependent Zeeman shift γB . In the rotating-wave approximation, the laboratory-frame Hamiltonian reads

$$H(B) = \omega_c a^\dagger a + \frac{\omega_q}{2} \sigma_z + g(a\sigma_+ + a^\dagger\sigma_-) + \frac{\gamma B}{2} \sigma_z, \quad (\text{B1})$$

with $\hbar = 1$ and the usual Pauli and ladder operators $\sigma_z = |e\rangle\langle e| - |g\rangle\langle g|$, $\sigma_+ = |e\rangle\langle g|$, $\sigma_- = |g\rangle\langle e|$.

We prepare the initial state

$$|\psi(0)\rangle = |e, 0\rangle, \quad (\text{B2})$$

and assume that throughout the relevant evolution time the dynamics remains in the single-excitation manifold spanned by $\{|e, 0\rangle, |g, 1\rangle\}$. In this manifold the total excitation number

$$N = a^\dagger a + \sigma_+ \sigma_- \quad (\text{B3})$$

is conserved and equals 1.

In the ordered basis $\{|e, 0\rangle, |g, 1\rangle\}$ we have the matrix representations

$$\begin{aligned} a^\dagger a &\mapsto \begin{pmatrix} 0 & 0 \\ 0 & 1 \end{pmatrix}, & \sigma_z &\mapsto \begin{pmatrix} 1 & 0 \\ 0 & -1 \end{pmatrix}, \\ a\sigma_+ + a^\dagger\sigma_- &\mapsto \begin{pmatrix} 0 & 1 \\ 1 & 0 \end{pmatrix}. \end{aligned} \quad (\text{B4})$$

Define the detuning

$$\Delta(B) := \omega_q + \gamma B - \omega_c, \quad (\text{B5})$$

and subtract the scalar term $(\omega_c/2)\mathbb{I}$ from $H(B)$: this does not affect any QFI element or variance, since adding $c\mathbb{I}$ to a Hamiltonian leaves commutators and variances invariant. We thus work with the traceless effective two-level Hamiltonian

$$H'(B) = g\tau_x + \frac{\Delta(B)}{2}\tau_z, \quad (\text{B6})$$

where $\boldsymbol{\tau} = (\tau_x, \tau_y, \tau_z)$ are Pauli matrices acting on $\{|e, 0\rangle, |g, 1\rangle\}$. Introducing the generalized Rabi frequency

$$\Omega(B) := \sqrt{\Delta(B)^2 + 4g^2}, \quad (\text{B7})$$

we can write

$$H'(B) = \frac{\Omega(B)}{2} \mathbf{n}(B) \cdot \boldsymbol{\tau}, \quad \mathbf{n}(B) = \frac{1}{\Omega(B)} (2g, 0, \Delta(B)). \quad (\text{B8})$$

The unitary time evolution in this manifold is

$$U(t; B) = e^{-iH'(B)t}. \quad (\text{B9})$$

The initial state $|\psi(0)\rangle = |e, 0\rangle$ is the +1 eigenstate of τ_z , which we denote by $|+z\rangle$ in what follows.

Local generators and QFI for (t, B)

For a pure state family $|\psi(x)\rangle = U(x)|\psi_0\rangle$ with parameters x^μ , the SLD QFIM is given by the covariance of the local generators G_μ defined by

$$i\partial_\mu U(x) = G_\mu(x)U(x). \quad (\text{B10})$$

Explicitly [6],

$$F_{\mu\nu} = 4\text{Cov}_{\psi_0}(G_\mu, G_\nu) := 4\text{Re}\left(\langle\psi_0|G_\mu G_\nu|\psi_0\rangle\langle\psi_0|G_\mu G_\nu|\psi_0\rangle - \langle\psi_0|G_\mu|\psi_0\rangle\langle\psi_0|G_\nu|\psi_0\rangle\right), \quad (\text{B11})$$

where all expectations are taken in the initial state $|\psi_0\rangle = |+z\rangle$.

In our case the parameters are (t, B) and

$$U(t, B) = e^{-iH'(B)t}. \quad (\text{B12})$$

The time generator is simply the Hamiltonian,

$$G_t = H'(B). \quad (\text{B13})$$

The field generator $G_B(t)$ is obtained by differentiating $U(t; B)$ with respect to B :

$$\begin{aligned} \partial_B U(t; B) &= -i \int_0^t U(t; B) U^\dagger(s; B) \partial_B H'(B) U(s; B) ds \\ &= -i U(t; B) \int_0^t U^\dagger(s; B) \partial_B H'(B) U(s; B) ds. \end{aligned} \quad (\text{B14})$$

Thus the local generator for B is

$$G_B(t) = \int_0^t U^\dagger(s; B) \partial_B H'(B) U(s; B) ds. \quad (\text{B15})$$

From (B6), the B -dependence enters only through the detuning, so that

$$\partial_B H'(B) = \frac{\gamma}{2} \tau_z. \quad (\text{B16})$$

Substituting (B16) into (B15) gives

$$G_B(t) = \frac{\gamma}{2} \int_0^t \tau_z(s) ds, \quad \tau_z(s) := U^\dagger(s; B) \tau_z U(s; B). \quad (\text{B17})$$

We therefore need the exact Heisenberg evolution of τ_z under H' .

The relevant moments in the initial state $|+z\rangle$ are

$$\begin{aligned} \langle \tau_z \rangle &= 1, & \langle \tau_x \rangle &= \langle \tau_y \rangle = 0, \\ \langle \tau_i \tau_j \rangle &= \delta_{ij}, & \text{Re} \langle \tau_i \tau_j \rangle &= 0 \quad (i \neq j), \end{aligned} \quad (\text{B18})$$

which we will use repeatedly below.

Heisenberg evolution of τ_z and closed-form $G_B(t)$

The effective Hamiltonian (B8) shows that the dynamics is a rotation on the Bloch sphere about the axis $\mathbf{n}(B)$ with angular frequency $\Omega(B)$. For any vector $\mathbf{v} \in \mathbb{R}^3$,

$$e^{+i(\Omega/2)\mathbf{n}\cdot\boldsymbol{\tau}s} (\mathbf{v}\cdot\boldsymbol{\tau}) e^{-i(\Omega/2)\mathbf{n}\cdot\boldsymbol{\tau}s} = (R_{\mathbf{n}}(\Omega s)\mathbf{v})\cdot\boldsymbol{\tau}, \quad (\text{B19})$$

where $R_{\mathbf{n}}(\theta)$ is the rotation matrix about \mathbf{n} by angle θ . Applying (B19) to $\mathbf{v} = \hat{z}$ yields

$$\tau_z(s) = v_x(s) \tau_x + v_y(s) \tau_y + v_z(s) \tau_z, \quad (\text{B20})$$

with coefficients determined by Rodrigues' formula

$$R_{\mathbf{n}}(\theta)\mathbf{v} = \mathbf{n}(\mathbf{n}\cdot\mathbf{v}) + (\mathbf{v} - \mathbf{n}\mathbf{n}\cdot\mathbf{v}) \cos \theta + (\mathbf{n} \times \mathbf{v}) \sin \theta. \quad (\text{B21})$$

Using $\mathbf{n} = (2g/\Omega, 0, \Delta/\Omega)$ and $\mathbf{v} = \hat{z}$, a straightforward calculation gives

$$\begin{aligned} v_x(s) &= \frac{2g\Delta}{\Omega^2} (1 - \cos \Omega s), \\ v_y(s) &= -\frac{2g}{\Omega} \sin \Omega s, \\ v_z(s) &= \frac{\Delta^2}{\Omega^2} + \frac{4g^2}{\Omega^2} \cos \Omega s, \end{aligned} \quad (\text{B22})$$

where we suppress the explicit B -dependence of Δ and Ω for readability.

Inserting (B20) and (B22) into (B17), we obtain

$$G_B(t) = \frac{\gamma}{2} \left(A_x(t) \tau_x + A_y(t) \tau_y + A_z(t) \tau_z \right), \quad (\text{B23})$$

with the time-dependent coefficients

$$A_x(t) = \int_0^t v_x(s) ds = \frac{2g\Delta}{\Omega^2} \left(t - \frac{\sin \Omega t}{\Omega} \right), \quad (\text{B24})$$

$$A_y(t) = \int_0^t v_y(s) ds = -\frac{2g}{\Omega^2} (1 - \cos \Omega t), \quad (\text{B25})$$

$$A_z(t) = \int_0^t v_z(s) ds = \frac{\Delta^2}{\Omega^2} t + \frac{4g^2}{\Omega^3} \sin \Omega t. \quad (\text{B26})$$

No approximations have been made: the only step between (B20) and (B24)–(B26) is the evaluation of elementary trigonometric integrals.

Exact QFIM entries F_{tt} , F_{BB} , and F_{tB}

We now evaluate the QFIM elements for the parameter pair (t, B) using (B11) and the local generators (B13) and (B23), with expectations taken in the initial state $|+z\rangle$.

(i) *The time-time element F_{tt} .* From (B6) and (B18),

$$\begin{aligned} \text{Var}(H') &= \left\langle \left(g\tau_x + \frac{\Delta}{2}\tau_z \right)^2 \right\rangle - \left\langle g\tau_x + \frac{\Delta}{2}\tau_z \right\rangle^2 \\ &= g^2 \langle \tau_x^2 \rangle + \frac{\Delta^2}{4} \langle \tau_z^2 \rangle + g\Delta \text{Re} \langle \tau_x \tau_z \rangle - \left(0 + \frac{\Delta}{2} \cdot 1 \right)^2 \\ &= g^2 + \frac{\Delta^2}{4} - \frac{\Delta^2}{4} = g^2, \end{aligned} \quad (\text{B27})$$

so that

$$F_{tt} = 4 \text{Var}(H') = 4g^2. \quad (\text{B28})$$

Equivalently, one may note that $(H')^2 = (\Delta^2/4 + g^2)\mathbb{I}$, so the variance in a pure state reduces to g^2 .

(ii) *The field-field element F_{BB} .* For any vector $\mathbf{b} \in \mathbb{R}^3$, $(\mathbf{b} \cdot \boldsymbol{\tau})^2 = \|\mathbf{b}\|^2 \mathbb{I}$, as the antisymmetric part drops out, and hence

$$\langle G_B^2 \rangle = \left(\frac{\gamma}{2} \right)^2 \langle (A_x \tau_x + A_y \tau_y + A_z \tau_z)^2 \rangle = \left(\frac{\gamma}{2} \right)^2 (A_x^2 + A_y^2 + A_z^2), \quad (\text{B29})$$

$$\langle G_B \rangle = \frac{\gamma}{2} (A_x \langle \tau_x \rangle + A_y \langle \tau_y \rangle + A_z \langle \tau_z \rangle) = \frac{\gamma}{2} A_z, \quad (\text{B30})$$

where we used (B18). Therefore

$$\text{Var}(G_B) = \langle G_B^2 \rangle - \langle G_B \rangle^2 = \left(\frac{\gamma}{2} \right)^2 (A_x^2 + A_y^2), \quad (\text{B31})$$

and

$$F_{BB}(t) = 4 \text{Var}(G_B) = \gamma^2 [A_x(t)^2 + A_y(t)^2]. \quad (\text{B32})$$

Substituting (B24) and (B25), we obtain the explicit closed form

$$\begin{aligned} F_{BB}(t) &= \frac{4g^2\gamma^2}{\Omega^4} \left[\Delta^2 \left(t - \frac{\sin \Omega t}{\Omega} \right)^2 + \left(1 - \cos \Omega t \right)^2 \right] \\ &= \frac{4g^2\gamma^2}{\Omega^4} \left[\Delta^2 \left(t - \frac{\sin \Omega t}{\Omega} \right)^2 + 4 \sin^4 \left(\frac{\Omega t}{2} \right) \right]. \end{aligned} \quad (\text{B33})$$

(iii) *The mixed element F_{tB} .* By (B11), the mixed QFI element is

$$F_{tB} = 4 \text{Cov}(H', G_B) = 4 \text{Re}(\langle H' G_B \rangle - \langle H' \rangle \langle G_B \rangle). \quad (\text{B34})$$

Using $H' = g\tau_x + (\Delta/2)\tau_z$ and G_B from (B23), with expectations in $|+z\rangle$,

$$\begin{aligned} \text{Cov}(H', G_B) &= \frac{\gamma}{2} \text{Re} \langle (g\tau_x + \frac{\Delta}{2}\tau_z) (A_x \tau_x + A_y \tau_y + A_z \tau_z) \rangle - \frac{\gamma}{2} \left(\frac{\Delta}{2} \right) A_z \\ &= \frac{\gamma}{2} \text{Re} (gA_x \langle \tau_x \tau_x \rangle + gA_y \langle \tau_x \tau_y \rangle + \frac{\Delta}{2} A_z \langle \tau_z \tau_z \rangle) - \frac{\gamma}{2} \frac{\Delta}{2} A_z. \end{aligned} \quad (\text{B35})$$

Using (B18), $\langle \tau_x \tau_x \rangle = \langle \tau_z \tau_z \rangle = 1$ and $\text{Re} \langle \tau_x \tau_y \rangle = 0$, we get

$$\text{Cov}(H', G_B) = \frac{\gamma}{2} g A_x. \quad (\text{B36})$$

Therefore

$$F_{tB}(t) = 4 \text{Cov}(H', G_B) = 2\gamma g A_x(t) = \frac{4g^2\gamma\Delta}{\Omega^2} \left(t - \frac{\sin \Omega t}{\Omega} \right). \quad (\text{B37})$$

Collecting the results (B28), (B33), and (B37), the full 2×2 QFIM for (t, B) is

$$F_{tt} = 4g^2, \quad (\text{B38})$$

$$F_{BB}(t) = \frac{4g^2\gamma^2}{\Omega^4} \left[\Delta^2 \left(t - \frac{\sin \Omega t}{\Omega} \right)^2 + 4 \sin^4 \left(\frac{\Omega t}{2} \right) \right], \quad (\text{B39})$$

$$F_{tB}(t) = \frac{4g^2\gamma\Delta}{\Omega^2} \left(t - \frac{\sin \Omega t}{\Omega} \right), \quad (\text{B40})$$

with $\Omega = \sqrt{\Delta^2 + 4g^2}$ and $\Delta = \omega_q + \gamma B - \omega_c$.

Schur-complement effective information $F_{\text{eff}}(t)$

We now treat t as the parameter of interest and B as a nuisance, and apply the Schur complement of Appendix A to obtain the effective information for time. With a single nuisance parameter, the Schur complement reduces to

$$F_{\text{eff}}(t) = F_{tt} - \frac{F_{tB}(t)^2}{F_{BB}(t)}, \quad (\text{B41})$$

understanding F_{BB}^{-1} as the Moore–Penrose pseudoinverse when $F_{BB} = 0$ (in which case necessarily $F_{tB} = 0$ as well). Substituting (B38)–(B40) and using A_x and A_y defined in (B24)–(B25), it is convenient to write $F_{BB} = \gamma^2(A_x^2 + A_y^2)$ and $F_{tB} = 2\gamma g A_x$. Then

$$\begin{aligned} F_{\text{eff}}(t) &= 4g^2 - \frac{4\gamma^2 g^2 A_x(t)^2}{\gamma^2(A_x(t)^2 + A_y(t)^2)} \\ &= 4g^2 \frac{A_y(t)^2}{A_x(t)^2 + A_y(t)^2}. \end{aligned} \quad (\text{B42})$$

Using the explicit expressions for A_x and A_y ,

$$A_x(t) = \frac{2g\Delta}{\Omega^2} \left(t - \frac{\sin \Omega t}{\Omega} \right), \quad (\text{B43})$$

$$A_y(t) = -\frac{2g}{\Omega^2} (1 - \cos \Omega t), \quad (\text{B44})$$

we can write $F_{\text{eff}}(t)$ in closed form:

$$\begin{aligned} F_{\text{eff}}(t) &= 4g^2 \frac{(1 - \cos(\Omega t))^2}{\Delta^2 \left(t - \frac{\sin(\Omega t)}{\Omega} \right)^2 + (1 - \cos(\Omega t))^2} \\ &= 4g^2 \frac{4 \sin^4\left(\frac{\Omega t}{2}\right)}{\Delta^2 \left(t - \frac{\sin(\Omega t)}{\Omega} \right)^2 + 4 \sin^4\left(\frac{\Omega t}{2}\right)}. \end{aligned} \quad (\text{B45})$$

By construction, $0 \leq F_{\text{eff}}(t) \leq F_{tt} = 4g^2$, and equality $F_{\text{eff}}(t) = 4g^2$ holds whenever $A_x(t) = 0$, i.e., when the mixed block F_{tB} vanishes.

The instantaneous projected speed is then

$$v_{\text{quo}}(t) = \frac{1}{2} \sqrt{F_{\text{eff}}(t)} = g \sqrt{\frac{A_y(t)^2}{A_x(t)^2 + A_y(t)^2}}, \quad (\text{B46})$$

and the time-averaged projected speed is

$$\bar{v}_{\text{quo}} = \frac{1}{\tau} \int_0^\tau \frac{1}{2} \sqrt{F_{\text{eff}}(t)} dt. \quad (\text{B47})$$

Fidelity, Bures angle, and quotient distance

To connect the effective information to an operational distance, we compute the fidelity between the initial state $|\psi(0)\rangle = |+\rangle$ and the evolved state $|\psi(t, B)\rangle = U(t; B)|+\rangle$. Using $H' = \frac{\Omega}{2} \mathbf{n} \cdot \boldsymbol{\tau}$ and (B8), the propagator is

$$U(t; B) = e^{-i\frac{\Omega t}{2} \mathbf{n} \cdot \boldsymbol{\tau}} = \cos \frac{\Omega t}{2} \mathbb{I} - i \sin \frac{\Omega t}{2} \mathbf{n} \cdot \boldsymbol{\tau}, \quad (\text{B48})$$

with $\mathbf{n} = (2g, 0, \Delta)/\Omega$. The overlap with $|+\rangle$ is

$$\begin{aligned} \langle \psi(0) | \psi(t, B) | \psi(0) | \psi(t, B) \rangle &= \langle +z | U(t; B) | +z \rangle \langle +z | U(t; B) | +z \rangle \\ &= \cos \frac{\Omega t}{2} - i \frac{\Delta}{\Omega} \sin \frac{\Omega t}{2}, \end{aligned} \quad (\text{B49})$$

where we used $\langle +z|\mathbf{n}\cdot\boldsymbol{\tau}|+z\rangle = n_z = \Delta/\Omega$. The fidelity is therefore

$$\begin{aligned} F(t, B) &= |\langle \psi(0)|\psi(t, B)\rangle|^2 \\ &= \cos^2 \frac{\Omega t}{2} + \left(\frac{\Delta}{\Omega}\right)^2 \sin^2 \frac{\Omega t}{2} \\ &= 1 - \frac{4g^2}{\Omega^2} \sin^2\left(\frac{\Omega t}{2}\right). \end{aligned} \quad (\text{B50})$$

This is the closed-system survival fidelity for the JC sensor at detuning $\Delta(B)$.

When B is treated as a nuisance, the relevant distance on the quotient manifold is obtained by optimizing the fidelity over admissible B values at fixed interrogation time τ . The quotient Bures angle is

$$\Theta_{\text{quo}}^{(\text{uni})}(\tau) := \arccos\left(\sup_{B \in \mathcal{B}} \sqrt{F(\tau, B)}\right), \quad (\text{B51})$$

where \mathcal{B} is the experimentally admissible set of fields (set by calibration and hardware constraints). Using (B50), this can be written as

$$\Theta_{\text{quo}}^{(\text{uni})}(\tau) = \arccos\left(\sqrt{1 - \inf_{B \in \mathcal{B}} \frac{4g^2}{\Omega(B)^2} \sin^2\left(\frac{\Omega(B)\tau}{2}\right)}\right). \quad (\text{B52})$$

If some $B \in \mathcal{B}$ satisfies $\Omega(B)\tau \in 2\pi\mathbb{Z}$, the infimum evaluates to 0 and $\Theta_{\text{quo}}^{(\text{uni})}(\tau) = 0$, reflecting the fact that the field may be chosen to bring the system back to its initial state at time τ .

The projected QSL then reads

$$\tau \geq \frac{\Theta_{\text{quo}}^{(\text{uni})}(\tau)}{\bar{v}_{\text{quo}}}, \quad (\text{B53})$$

with \bar{v}_{quo} given by (B47). This is the closed-system counterpart of the general projected QSL of Appendix A.

Short-time expansion and detuning tolerances

For short evolution times where $|\Omega t| \ll 1$ and $|\Delta t| \ll 1$, the ratio of the effective to the physical Fisher information admits a simple approximate expression that quantifies the impact of detuning on the projected speed. From (B42),

$$\frac{F_{\text{eff}}(t)}{F_{tt}} = \frac{A_y(t)^2}{A_x(t)^2 + A_y(t)^2}, \quad (\text{B54})$$

with A_x and A_y given by (B24)–(B25). Expanding

$$\sin(\Omega t) \approx \Omega t - \frac{(\Omega t)^3}{6}, \quad \cos(\Omega t) \approx 1 - \frac{(\Omega t)^2}{2}, \quad (\text{B55})$$

we obtain to leading nontrivial orders

$$A_y(t) = -\frac{2g}{\Omega^2}(1 - \cos \Omega t) \approx -\frac{2g}{\Omega^2} \frac{(\Omega t)^2}{2} = -g t^2 + O(t^4), \quad (\text{B56})$$

$$A_x(t) = \frac{2g\Delta}{\Omega^2} \left(t - \frac{\sin \Omega t}{\Omega}\right) \approx \frac{2g\Delta}{\Omega^2} \frac{(\Omega t)^3}{6} = \frac{g\Delta}{3} t^3 + O(t^5). \quad (\text{B57})$$

Therefore

$$\frac{A_x(t)^2}{A_y(t)^2} \approx \frac{((g\Delta/3)t^3)^2}{(gt^2)^2} = \left(\frac{\Delta t}{3}\right)^2, \quad (\text{B58})$$

and substituting into (B54) gives

$$\frac{F_{\text{eff}}(t)}{F_{tt}} = \frac{1}{1 + A_x^2/A_y^2} \approx \frac{1}{1 + (\Delta t/3)^2}. \quad (\text{B59})$$

Thus, at short times the projected (effective) speed satisfies

$$\frac{v_{\text{quo}}(t)}{\frac{1}{2}\sqrt{F_{tt}}} = \sqrt{\frac{F_{\text{eff}}(t)}{F_{tt}}} \approx \frac{1}{\sqrt{1 + (\Delta t/3)^2}}, \quad (\text{B60})$$

showing that any nonzero detuning reduces the operational speed, with a quadratic penalty in the product $|\Delta|t$.

To maintain the effective information at a fraction $R \in (0, 1]$ of the physical one (i.e., $F_{\text{eff}}/F_{tt} \geq R$), the short-time approximation (B59) implies the tolerance condition

$$\frac{1}{1 + (\Delta t/3)^2} \geq R \implies |\Delta|t < 3\sqrt{\frac{1}{R} - 1}. \quad (\text{B61})$$

This sets a quantitative requirement on how close to resonance the system must be kept for a given interrogation time t in order to retain a target fraction R of the physical QSL speed.

For example, using (B61), one finds

Retention R	Tolerance condition on $ \Delta t$
$R = 0.99$	$ \Delta t < 0.30$
$R = 0.95$	$ \Delta t < 0.69$
$R = 0.90$	$ \Delta t < 1.00$

valid in the regime $|\Delta|t \lesssim 1$. These relations can be used to translate metrological design targets (e.g., “retain at least 95% of the speed-limit tightness”) into concrete specifications on detuning control, calibration effort, and maximal interrogation time for the JC sensor.

APPENDIX C: OPEN JAYNES–CUMMINGS SENSOR — DISPERSIVE LOSSY CASE

In this section, we embed the projected speed-limit formalism of Appendix A into a realistic open Jaynes–Cummings (JC) sensor operating in the dispersive regime. We (i) specify the full atom–cavity Hamiltonian with Markovian dissipation; (ii) carry out a Schrieffer–Wolff (dispersive) transformation of both the Hamiltonian and the Lindblad operators, making all approximations explicit; (iii) derive an effective master equation for a truncated cavity qubit with a field-dependent frequency and Purcell-enhanced decay rate; (iv) solve this reduced dynamics exactly in Bloch form; (v) compute the quantum Fisher information (QFI) for laboratory time t and field B , together with the mixed element F_{tB} ; and (vi) build the Schur-complement effective information $F_{\text{eff}}(t)$ and the corresponding projected (quotient) QSL.

Throughout this Appendix we work in units $\hbar = 1$.

Full JC model with Markovian dissipation

We consider a two-level atom (or qubit) with ground and excited states $|g\rangle$ and $|e\rangle$, coupled to a single cavity mode truncated to the lowest two Fock states $\{|0\rangle, |1\rangle\}$. The total Hilbert space is

$$\mathcal{H} = \mathcal{H}_{\text{cav}}^{(2)} \otimes \mathcal{H}_{\text{atom}} = \text{span}\{|0\rangle, |1\rangle\} \otimes \text{span}\{|g\rangle, |e\rangle\}. \quad (\text{C1})$$

On the truncated cavity space we use

$$\tilde{a} = |0\rangle\langle 1|, \quad \tilde{a}^\dagger = |1\rangle\langle 0|, \quad \tilde{a}^\dagger \tilde{a} = |1\rangle\langle 1|. \quad (\text{C2})$$

The atomic operators are the usual Pauli matrices $\sigma_z = |e\rangle\langle e| - |g\rangle\langle g|$ and $\sigma_+ = |e\rangle\langle g|$, $\sigma_- = |g\rangle\langle e|$.

The laboratory-frame Hamiltonian in the rotating-wave approximation is

$$H = \omega_c \tilde{a}^\dagger \tilde{a} + \frac{\omega'_a(B)}{2} \sigma_z + g(\sigma_+ \tilde{a} + \sigma_- \tilde{a}^\dagger), \quad (\text{C3})$$

with cavity frequency ω_c , atom–cavity coupling g , and a field-dependent atomic transition frequency

$$\omega'_a(B) = \omega_a + \eta B, \quad (\text{C4})$$

where η is a Zeeman coefficient (e.g. $\eta = 2\mu_B$ in suitable units). The magnetic field B is the sensing parameter.

Dissipation is described by a GKSL generator with three Markovian channels:

$$\begin{aligned} L_\kappa &= \sqrt{\kappa} \tilde{a} && \text{(cavity loss),} \\ L_{\gamma_1} &= \sqrt{\gamma_1} \sigma_- && \text{(atomic relaxation),} \\ L_{\gamma_\varphi} &= \sqrt{\gamma_\varphi/2} \sigma_z && \text{(atomic dephasing).} \end{aligned} \quad (\text{C5})$$

The full master equation is

$$\dot{\rho} = -i[H, \rho] + \kappa \mathcal{D}[\tilde{a}]\rho + \gamma_1 \mathcal{D}[\sigma_-]\rho + \gamma_\varphi \mathcal{D}[\sigma_z]\rho, \quad (\text{C6})$$

where the dissipator is

$$\mathcal{D}[L]\rho := L\rho L^\dagger - \frac{1}{2}\{L^\dagger L, \rho\}. \quad (\text{C7})$$

This is of the GKSL form $\dot{\rho} = \mathcal{L}_B[\rho]$ used in Appendix A, with B the nuisance parameter and t the laboratory time.

We work in the dispersive regime

$$|\Delta(B)| \gg g, \quad \Delta(B) := \omega_c - \omega'_a(B), \quad (\text{C8})$$

and keep terms up to second order in the small parameter $\lambda := g/\Delta(B)$ when performing the dispersive transformation.

Dispersive (Schrieffer–Wolff) transformation

To eliminate the transverse coupling and expose the dispersive shift and Purcell effect, we implement a Schrieffer–Wolff transformation generated by

$$S = \lambda(\sigma_+ \tilde{a} - \sigma_- \tilde{a}^\dagger), \quad \lambda = \frac{g}{\Delta(B)}. \quad (\text{C9})$$

The unitary transformation is $T = e^S$. The transformed Hamiltonian is

$$H' = e^{-S} H e^S \approx H + [H, S] + \frac{1}{2}[[H, S], S], \quad (\text{C10})$$

where we keep terms up to $O(\lambda^2)$.

A straightforward but standard calculation (see e.g. [33, 34]) gives the dispersive Hamiltonian

$$H' = \omega_c \tilde{a}^\dagger \tilde{a} + \frac{1}{2}[\omega'_a(B) + \chi(B)]\sigma_z + \chi(B)\sigma_z \tilde{a}^\dagger \tilde{a}, \quad (\text{C11})$$

with the AC Stark (dispersive) shift

$$\chi(B) = \frac{g^2}{\Delta(B)}. \quad (\text{C12})$$

Equation (C11) removes the transverse coupling to leading order, replacing it with a state-dependent cavity frequency and a state-dependent atomic frequency.

Polaron-transformed dissipators and Purcell channel

The dispersive transformation must also be applied to the Lindblad operators. For any system operator L , we define

$$L' := T^\dagger L T \approx L + [L, S] + O(\lambda^2). \quad (\text{C13})$$

Retaining terms to first order in λ gives the leading corrections generated by the atom–cavity coupling inside the dissipators.

Cavity loss. For $L_\kappa = \sqrt{\kappa} \tilde{a}$,

$$\begin{aligned} [L_\kappa, S] &= [\sqrt{\kappa} \tilde{a}, \lambda(\sigma_+ \tilde{a} - \sigma_- \tilde{a}^\dagger)] \\ &= -\lambda \sqrt{\kappa} \sigma_- [\tilde{a}, \tilde{a}^\dagger] \\ &= -\lambda \sqrt{\kappa} \sigma_-. \end{aligned} \quad (\text{C14})$$

Thus

$$L'_\kappa \approx \sqrt{\kappa} (\tilde{a} + \lambda \sigma_-). \quad (\text{C15})$$

Physically, cavity loss now induces an additional decay path for the atom.

Atomic relaxation. For $L_{\gamma_1} = \sqrt{\gamma_1} \sigma_-$,

$$\begin{aligned} [L_{\gamma_1}, S] &= [\sqrt{\gamma_1} \sigma_-, \lambda(\sigma_+ \tilde{a} - \sigma_- \tilde{a}^\dagger)] \\ &= \sqrt{\gamma_1} \lambda [\sigma_-, \sigma_+] \tilde{a} \\ &= -\sqrt{\gamma_1} \lambda \sigma_z \tilde{a}. \end{aligned} \quad (\text{C16})$$

Hence

$$L'_{\gamma_1} \approx \sqrt{\gamma_1} (\sigma_- - \lambda \sigma_z \tilde{a}), \quad (\text{C17})$$

which couples the atomic relaxation channel to the cavity field.

Atomic dephasing. For $L_{\gamma_\varphi} = \sqrt{\gamma_\varphi/2} \sigma_z$,

$$\begin{aligned} [L_{\gamma_\varphi}, S] &= \left[\sqrt{\frac{\gamma_\varphi}{2}} \sigma_z, \lambda(\sigma_+ \tilde{a} - \sigma_- \tilde{a}^\dagger) \right] \\ &= \sqrt{\frac{\gamma_\varphi}{2}} \lambda \left([\sigma_z, \sigma_+] \tilde{a} - [\sigma_z, \sigma_-] \tilde{a}^\dagger \right) \\ &= \sqrt{\frac{\gamma_\varphi}{2}} \lambda \left(2\sigma_+ \tilde{a} + 2\sigma_- \tilde{a}^\dagger \right). \end{aligned} \quad (\text{C18})$$

Thus

$$L'_{\gamma_\varphi} \approx \sqrt{\gamma_\varphi/2} \left(\sigma_z - 2\lambda(\sigma_+ \tilde{a} + \sigma_- \tilde{a}^\dagger) \right), \quad (\text{C19})$$

which generates dephasing-induced excitation exchange between atom and cavity.

Approximation hierarchy. A fully rigorous treatment would keep all first-order corrections in (C15), (C17), (C19) inside the dissipators $\mathcal{D}[L'_\kappa]$, $\mathcal{D}[L'_{\gamma_1}]$, $\mathcal{D}[L'_{\gamma_\varphi}]$. In many dispersive experiments, however, one operates in a parameter regime where

$$\kappa \lambda^2 \ll \gamma_1, \quad \gamma_\varphi \lambda^2 \ll \gamma_1, \quad (\text{C20})$$

so that the cavity-induced corrections to the κ and γ_φ channels are negligible compared to the dominant atomic relaxation. In this case one can safely neglect the λ corrections in L'_κ and L'_{γ_φ} , while keeping the leading $O(\lambda^2)$ Purcell term generated by L'_{γ_1} .

Concretely, inserting L'_{γ_1} into $\mathcal{D}[L'_{\gamma_1}]$ gives

$$\mathcal{D}[L'_{\gamma_1}] \rho' = \gamma_1 \mathcal{D}[\sigma_-] \rho' - \gamma_1 \lambda \mathcal{K}[\sigma_-, \sigma_z \tilde{a}] \rho' + \gamma_1 \lambda^2 \mathcal{D}[\sigma_z \tilde{a}] \rho', \quad (\text{C21})$$

where \mathcal{K} denotes the interference superoperator. Under the usual assumption that the interference term averages out in observables (e.g. on timescales relevant for cavity dynamics), the dominant correction is the second-order term, which yields an additional decay channel for the cavity via atomic relaxation: the Purcell effect.

Within these approximations, the transformed master equation reads

$$\begin{aligned} \dot{\rho}' &\approx -i[H', \rho'] + \kappa \mathcal{D}[\tilde{a}] \rho' + \gamma_1 \mathcal{D}[\sigma_-] \rho' \\ &\quad + \gamma_1 \lambda^2 \mathcal{D}[\sigma_z \tilde{a}] \rho' + \gamma_\varphi \mathcal{D}[\sigma_z] \rho', \end{aligned} \quad (\text{C22})$$

with H' as in (C11).

Reduced cavity master equation and effective parameters

We now trace out the atomic degree of freedom under the assumption that the atom relaxes rapidly to a diagonal state with inversion

$$\langle \sigma_z \rangle = p_e - p_g, \quad p_e + p_g = 1, \quad (\text{C23})$$

on the timescale of interest for the cavity dynamics. This is justified when γ_1 is large compared to the effective cavity decay rate.

The coherent part of (C22) gives

$$\text{Tr}_{\text{atom}}(-i[H', \rho']) = -i[(\omega_c + \chi(B)\langle \sigma_z \rangle)\tilde{a}^\dagger \tilde{a}, \rho_{\text{cav}}], \quad (\text{C24})$$

where $\rho_{\text{cav}} := \text{Tr}_{\text{atom}}\rho'$ is the reduced cavity state. Thus the cavity resonance frequency is shifted to

$$\omega'_c(B) := \omega_c + \chi(B)\langle \sigma_z \rangle. \quad (\text{C25})$$

The cavity loss channel $\kappa \mathcal{D}[\tilde{a}]\rho'$ reduces to the same form on the cavity. The Purcell term $\gamma_1 \lambda^2 \mathcal{D}[\sigma_z \tilde{a}]\rho'$ contributes an additional cavity dissipator $\propto \mathcal{D}[\tilde{a}]$ after tracing out the atom and inserting the inversion. Collecting these contributions, one arrives at the reduced cavity master equation

$$\begin{aligned} \dot{\rho}_{\text{cav}} = & -i[\omega'_c(B)\tilde{a}^\dagger \tilde{a}, \rho_{\text{cav}}] \\ & + \kappa_{\text{eff}}(B)\mathcal{D}[\tilde{a}]\rho_{\text{cav}}, \end{aligned} \quad (\text{C26})$$

with the field-dependent effective decay rate

$$\kappa_{\text{eff}}(B) = \kappa + \gamma_1 \left(\frac{g}{\Delta(B)} \right)^2. \quad (\text{C27})$$

The first term is the bare cavity loss, while the second is the Purcell contribution arising from atomic relaxation in the dispersive regime.

Equations (C25) and (C27) provide the B -dependence of the GKSL data $H(B)$ and $F_k(B)$ required to compute the QFIM blocks along the trajectory, in the notation of Appendix A.

Cavity qubit dynamics and Bloch-vector representation

We restrict the cavity to the $\{|0\rangle, |1\rangle\}$ subspace and prepare the initial pure state

$$|\psi_0\rangle = \cos\theta |0\rangle + \sin\theta |1\rangle, \quad (\text{C28})$$

with $\theta \in [0, \pi/2]$. After tracing out the atom, the initial cavity density matrix is

$$\rho_{\text{cav}}(0) = \begin{pmatrix} \cos^2\theta & \cos\theta \sin\theta \\ \cos\theta \sin\theta & \sin^2\theta \end{pmatrix}, \quad (\text{C29})$$

in the ordered basis $\{|0\rangle, |1\rangle\}$.

The master equation (C26) is that of a qubit subject to a phase rotation at frequency $\omega'_c(B)$ and amplitude damping at rate $\kappa_{\text{eff}}(B)$. Its exact solution is well-known and reads

$$\rho_{\text{cav}}(t; B) = \begin{pmatrix} 1 - \sin^2\theta e^{-\kappa_{\text{eff}}t} & \cos\theta \sin\theta e^{i\omega'_c t} e^{-\kappa_{\text{eff}}t/2} \\ \cos\theta \sin\theta e^{-i\omega'_c t} e^{-\kappa_{\text{eff}}t/2} & \sin^2\theta e^{-\kappa_{\text{eff}}t} \end{pmatrix}, \quad (\text{C30})$$

where, for brevity, we write $\omega'_c = \omega'_c(B)$ and $\kappa_{\text{eff}} = \kappa_{\text{eff}}(B)$.

Any qubit state can be written as

$$\rho_{\text{cav}}(t; B) = \frac{1}{2} [\mathbb{I} + \vec{S}(t; B) \cdot \vec{\sigma}], \quad (\text{C31})$$

with Pauli vector $\vec{\sigma} = (\sigma_x, \sigma_y, \sigma_z)$ and Bloch vector $\vec{S}(t; B) = (S_x, S_y, S_z)$. From (C30) we obtain

$$\begin{aligned} S_x(t; B) &= 2 \operatorname{Re} \rho_{01}(t; B) = \sin 2\theta \cos(\omega'_c t) e^{-\kappa_{\text{eff}} t/2}, \\ S_y(t; B) &= -2 \operatorname{Im} \rho_{01}(t; B) = -\sin 2\theta \sin(\omega'_c t) e^{-\kappa_{\text{eff}} t/2}, \\ S_z(t; B) &= \rho_{11}(t; B) - \rho_{00}(t; B) = 2 \sin^2 \theta e^{-\kappa_{\text{eff}} t} - 1. \end{aligned} \quad (\text{C32})$$

The time derivatives are

$$\begin{aligned} \dot{S}_x(t; B) &= -\sin 2\theta e^{-\kappa_{\text{eff}} t/2} \left[\omega'_c \sin(\omega'_c t) + \frac{\kappa_{\text{eff}}}{2} \cos(\omega'_c t) \right], \\ \dot{S}_y(t; B) &= -\sin 2\theta e^{-\kappa_{\text{eff}} t/2} \left[\omega'_c \cos(\omega'_c t) - \frac{\kappa_{\text{eff}}}{2} \sin(\omega'_c t) \right], \\ \dot{S}_z(t; B) &= -2\kappa_{\text{eff}} \sin^2 \theta e^{-\kappa_{\text{eff}} t}. \end{aligned} \quad (\text{C33})$$

We will also need the squared norm and dot product

$$|\dot{\vec{S}}(t; B)|^2 = \dot{S}_x^2 + \dot{S}_y^2 + \dot{S}_z^2, \quad \vec{S} \cdot \dot{\vec{S}} = S_x \dot{S}_x + S_y \dot{S}_y + S_z \dot{S}_z, \quad (\text{C34})$$

and

$$|\vec{S}(t; B)|^2 = S_x^2 + S_y^2 + S_z^2. \quad (\text{C35})$$

Fidelity between initial and time-evolved cavity states

The initial cavity state is pure, $\rho_0 = |\psi_0\rangle\langle\psi_0|$ with $|\psi_0\rangle$ given by (C28). The fidelity between ρ_0 and $\rho_{\text{cav}}(t; B)$ is therefore

$$F(\rho_0, \rho_{\text{cav}}(t; B)) = \langle\psi_0| \rho_{\text{cav}}(t; B) |\psi_0\rangle. \quad (\text{C36})$$

Writing $|\psi_0\rangle = (\cos \theta, \sin \theta)^\top$ in the $\{|0\rangle, |1\rangle\}$ basis and inserting (C30), one finds

$$\begin{aligned} F(\rho_0, \rho_{\text{cav}}(t; B)) &= \cos^2 \theta \rho_{00}(t; B) + \sin^2 \theta \rho_{11}(t; B) + 2 \cos \theta \sin \theta \operatorname{Re} \rho_{01}(t; B) \\ &= \cos^2 \theta \left[1 - \sin^2 \theta e^{-\kappa_{\text{eff}} t} \right] + \sin^4 \theta e^{-\kappa_{\text{eff}} t} \\ &\quad + 2 \cos^2 \theta \sin^2 \theta e^{-\kappa_{\text{eff}} t/2} \cos(\omega'_c t). \end{aligned} \quad (\text{C37})$$

Collecting terms,

$$\begin{aligned} F(\rho_0, \rho_{\text{cav}}(t; B)) &= \cos^2 \theta + \sin^4 \theta e^{-\kappa_{\text{eff}} t} - \cos^2 \theta \sin^2 \theta e^{-\kappa_{\text{eff}} t} \\ &\quad + 2 \cos^2 \theta \sin^2 \theta e^{-\kappa_{\text{eff}} t/2} \cos(\omega'_c t). \end{aligned} \quad (\text{C38})$$

This expression will enter the numerator of the projected QSL.

QFI for time and field; mixed element

For a general mixed qubit state with Bloch vector $\vec{S}(x)$ depending on a real parameter x , the SLD QFI is given by the standard formula

$$F_Q(x) = |\partial_x \vec{S}|^2 + \frac{(\vec{S} \cdot \partial_x \vec{S})^2}{1 - |\vec{S}|^2}, \quad |\vec{S}| < 1, \quad (\text{C39})$$

with the pure-state limit obtained by continuity as $|\vec{S}| \rightarrow 1$.

Time QFI. Taking $x = t$ with B fixed, we write

$$F_{tt}(t; B) := F_Q(t) = |\dot{\vec{S}}(t; B)|^2 + \frac{[\vec{S}(t; B) \cdot \dot{\vec{S}}(t; B)]^2}{1 - |\vec{S}(t; B)|^2}, \quad (\text{C40})$$

with \vec{S} and $\dot{\vec{S}}$ given by (C32)–(C33). This is the physical Bures speed squared (up to the factor 1/4) along the open-system trajectory for fixed field.

Field QFI. The field enters through the effective frequency $\omega'_c(B)$ and decay rate $\kappa_{\text{eff}}(B)$. It is convenient to denote

$$\Omega(B) := \omega'_c(B), \quad \Gamma(B) := \kappa_{\text{eff}}(B), \quad (\text{C41})$$

and their derivatives

$$\Omega'(B) := \partial_B \Omega(B), \quad \Gamma'(B) := \partial_B \Gamma(B). \quad (\text{C42})$$

From (C25) and (C27),

$$\Omega'(B) = \chi'(B) \langle \sigma_z \rangle = \langle \sigma_z \rangle \partial_B \left(\frac{g^2}{\Delta(B)} \right) = - \langle \sigma_z \rangle \frac{g^2 \Delta'(B)}{\Delta(B)^2}, \quad (\text{C43})$$

$$\Gamma'(B) = \partial_B \left[\kappa + \gamma_1 \left(\frac{g}{\Delta(B)} \right)^2 \right] = -2\gamma_1 \frac{g^2 \Delta'(B)}{\Delta(B)^3}, \quad (\text{C44})$$

with $\Delta'(B) = -\omega'_a(B)$ from (C4).

Differentiating (C32) with respect to B yields

$$\begin{aligned} \partial_B S_x &= -\sin 2\theta e^{-\Gamma t/2} \left[t\Omega' \sin(\Omega t) + \frac{t}{2}\Gamma' \cos(\Omega t) \right], \\ \partial_B S_y &= -\sin 2\theta e^{-\Gamma t/2} \left[t\Omega' \cos(\Omega t) - \frac{t}{2}\Gamma' \sin(\Omega t) \right], \\ \partial_B S_z &= -2\sin^2 \theta t\Gamma' e^{-\Gamma t}, \end{aligned} \quad (\text{C45})$$

where again $\Omega = \Omega(B)$ and $\Gamma = \Gamma(B)$.

The field QFI is then

$$F_{BB}(t; B) := F_Q(B; t) = |\partial_B \vec{S}(t; B)|^2 + \frac{[\vec{S}(t; B) \cdot \partial_B \vec{S}(t; B)]^2}{1 - |\vec{S}(t; B)|^2}, \quad (\text{C46})$$

with $|\partial_B \vec{S}|^2$ and $\vec{S} \cdot \partial_B \vec{S}$ evaluated using (C32) and (C45). This is the nuisance information needed in the Schur complement.

Mixed element. The mixed QFI element F_{tB} can be written in Bloch form as

$$F_{tB}(t; B) = \dot{\vec{S}}(t; B) \cdot \partial_B \vec{S}(t; B) + \frac{[\vec{S}(t; B) \cdot \dot{\vec{S}}(t; B)] [\vec{S}(t; B) \cdot \partial_B \vec{S}(t; B)]}{1 - |\vec{S}(t; B)|^2}. \quad (\text{C47})$$

Equations (C40), (C46), and (C47) provide the full 2×2 QFIM in the parameter pair (t, B) for the open, dispersive JC sensor.

Schur-complement information and projected QSL

Treating t as the parameter of interest and B as a nuisance, the effective information for time is given by the one-dimensional Schur complement

$$F_{\text{eff}}(t; B) = F_{tt}(t; B) - \frac{F_{tB}(t; B)^2}{F_{BB}(t; B)}, \quad (\text{C48})$$

with the understanding that F_{BB}^{-1} is interpreted as the Moore–Penrose pseudoinverse (and $F_{\text{eff}} = F_{tt}$) whenever $F_{BB} = 0$. By positive semidefiniteness of the QFIM, $F_{\text{eff}} \geq 0$, and $F_{\text{eff}} \leq F_{tt}$ with equality if and only if $F_{tB} = 0$.

The instantaneous projected (quotient) speed is

$$v_{\text{quo}}(t; B) = \frac{1}{2} \sqrt{F_{\text{eff}}(t; B)}, \quad (\text{C49})$$

and its time average over the interrogation interval $[0, \tau]$ is

$$\bar{v}_{\text{quo}}(B) = \frac{1}{\tau} \int_0^\tau \frac{1}{2} \sqrt{F_{\text{eff}}(t; B)} dt. \quad (\text{C50})$$

For a fixed field B , this reduces to the standard QSL denominator, but with the profiled speed rather than the physical one.

Because B is a nuisance parameter that may be re-tuned between experimental runs within an admissible set \mathcal{B} , the numerator must live on the quotient manifold in which states that differ only by a change in B are identified. The relevant Bures angle is therefore

$$\Theta_{\text{quo}}(\tau) := \arccos\left(\sup_{B \in \mathcal{B}} \sqrt{F(\rho_0, \rho_{\text{cav}}(\tau; B))}\right), \quad (\text{C51})$$

where $F(\rho_0, \rho_{\text{cav}}(\tau; B))$ is given explicitly in (C38).

The quotient angle is obtained by optimizing the explicit fidelity (C38) over the admissible calibration window \mathcal{B} . Define

$$\begin{aligned} F(B; \tau) &:= F(\rho_0, \rho_{\text{cav}}(\tau; B)) \\ &= \cos^2 \theta + \sin^4 \theta e^{-\kappa_{\text{eff}}(B)\tau} - \cos^2 \theta \sin^2 \theta e^{-\kappa_{\text{eff}}(B)\tau} \\ &\quad + 2 \cos^2 \theta \sin^2 \theta e^{-\kappa_{\text{eff}}(B)\tau/2} \cos(\omega'_c(B)\tau). \end{aligned} \quad (\text{C52})$$

Then Eq. (C51) becomes

$$\Theta_{\text{quo}}(\tau) = \arccos\left(\sup_{B \in \mathcal{B}} \sqrt{F(B; \tau)}\right). \quad (\text{C53})$$

Combining the quotient distance and the projected speed, the nuisance-profiled QSL for a fixed realized field value B in the open JC sensor reads

$$\tau \geq \frac{\Theta_{\text{quo}}(\tau)}{\frac{1}{\tau} \int_0^\tau \frac{1}{2} \sqrt{F_{tt}(t; B) - \frac{F_{tB}(t; B)^2}{F_{BB}(t; B)}} dt}, \quad (\text{C54})$$

with F_{tt} , F_{BB} , and F_{tB} given by (C40), (C46), and (C47), and $\Theta_{\text{quo}}(\tau)$ given by (C53).

If the dynamics is insensitive to B over the admissible range (e.g. $\Omega'(B) \equiv 0$ and $\Gamma'(B) \equiv 0$ so that $\partial_B \vec{S} \equiv 0$), then $F_{BB} = F_{tB} = 0$ and $F_{\text{eff}} = F_{tt}$. The quotient angle reduces to the physical Bures angle $L(\rho_0, \rho_{\text{cav}}(\tau; B))$ for any B , and (C54) collapses to the standard open-system QSL. If $F_{tB} \equiv 0$ while $F_{BB} > 0$, then $F_{\text{eff}} = F_{tt}$, so the projected and physical QSL denominators coincide for the same realized field value B_0 . The numerator remains profiled via $\Theta_{\text{quo}}(\tau) \leq \arccos \sqrt{F(\rho_0, \rho_{\text{cav}}(\tau; B_0))}$, because the quotient angle is obtained by maximizing the fidelity over the admissible calibration window before applying the decreasing function arccos. The projected QSL lower bound is therefore weaker than or equal to the corresponding physical QSL lower bound. In the limit $\kappa_{\text{eff}}\tau \ll 1$, $\Gamma'(B)\tau \ll 1$, and with detuning tolerance chosen such that the coherent dynamics dominates over decay, the open-system QFIM and projected QSL smoothly approach their closed-system counterparts of Appendix B)
